Elsevier Editorial System(tm) for Journal of Environmental Radioactivity

Manuscript Draft

Manuscript Number:

Title: Characterization and 10Be content of iron carbonate concretions for genetic aspects - Weathering, desert varnish or burning: rim effects in iron carbonate concretions

Article Type: SI: TREICEP2016

Keywords: iron-carbonate concretions, siderite, microbial, 10Be content, heated rim minerals, weathering vs. heating effects

Corresponding Author: Prof. Márta Polgári, D.Sc.

Corresponding Author's Institution: Research Center for Astronomy and Geosciences, Hungarian Academy of Sciences

First Author: Márta Polgári, D.Sc.

Order of Authors: Márta Polgári, D.Sc.; Szaniszló Bérczi, PhD; Kazuho Horiuchi, PhD; Hiroyuki Matsuzaki, PhD; Tibor Kovács, Prof.; Sándor Józsa, PhD; Zsolt Bendő, PhD; Krisztián Fintor, PhD; József Fekete, PhD; Zoltán Homonnay, Prof.; Ernő Kuzmann, Prof.; Arnold Gucsik, PhD; Ildikó Gyollai, PhD; János Kovács, PhD; István Dódony, Prof.

Abstract: Three iron carbonate (siderite) sedimentary concretions were investigated from Nagykovácsi, Uri and Délegyháza, Hungary. Comparative petrological, mineralogical, geochemical and isotopic studies were carried out on identifying possible source rocks and effects of the glaze-like exposed surface of the concretions. The samples are microbially mediated siderite concretions with embedded metamorphous and igneous mineral clasts, and have specific rim belts characterized by semi-concentric outer Fe-oxide layer, fluffy pyrite-rich outer belt and siderite inner part. The cross section of the Fe-carbonate concretions is investigated by independent methodologies in order to identify their rim effects. Their surficial oxide layers are witness of degassing of the exposed surface caused most probably by elevated temperatures. The inner rim pyrite belt in the concretions excludes longer staying in wet surface environment. Microtextural and mineralogical features do not support desert varnish formation. 10Be nuclide values of the Nagykovácsi and Uri concretions stand far over the level of terrestrial in situ cosmogenic nuclides, but they are in accord of the lowest region for meteorites. Though the data are not conclusive to confirm any kind of known origin, they are contradictional, and open possibilities for a scenario of terrestrial meteorite origin.

Characterization and ^{10}Be content of iron carbonate concretions for genetic aspects - Weathering, desert varnish or burning: rim effects in iron carbonate concretions

Márta Polgári[1,2*], Szaniszló Bérczi[3], Kazuho Horiuchi[4], Hiroyuki Matsuzaki[5], Tibor Kovács[6], Sándor Józsa[7], Zsolt Bendő[7], Krisztián Fintor[8], József Fekete[1], Zoltán Homonnay[9], Ernő Kuzmann[9], Arnold Gucsik[10], Ildikó Gyollai[1], János Kovács[11], István Dódony[12]

[1]*Research Center for Astronomy and Geosciences, Geobiomineralization and Astrobiological Research Group, Institute for Geology and Geochemistry, Hungarian Academy of Sciences, 1112 Budapest, Budaörsi út. 45, Hungary, e-mail: rodokrozit@gmail.com*
[2]*Eszterházy Károly University, Dept. of Physical Geography and Geoinformatics, Leányka str. 6, 3300 Eger, Hungary*
[3]*Eötvös University, Faculty of Science, Dept. of Materials Physics, Cosmic Materials Space Res. Group, 1117 Budapest, Pázmány P. s. 1/a. Hungary, e-mail: bercziszani@caesar.elte.hu*
[4]*Graduate School of Science and Technology, Hirosaki University, 3, Bunkyo-chou, Hirosaki, Aomori 036-8561, Japan, e-mmail: kh@cc.hirosaki-u.ac.jp*
[5]*Micro Analysis Laboratory, Tandem accelerator (MALT), The University Museum, The University of Tokyo, 2-11-16, Yayoi, Bunkyo-ku, Tokyo 113-0032, Japan, e-mail: hmatsu@um.u-tokyo.ac.jp*
[6]*Institute of Radiochemistry and Radioecology, University of Pannonia, Egyetem Str. 10, Veszprém, H-8200, Hungary, Phone: +36 88 624-789, Fax: +36 88 624-178, e-mail: kt@almos.uni-pannon.hu*
[7]*Eötvös University, Dept. Petrology and Geochemistry, 1117 Budapest, Pázmány P. s. 1/c.*
[8]*Szeged University, Department of Mineralogy, Geochemistry and Petrology, Egyetem str. 2-6, 6702 Szeged, Hungary, e-mail: palm@geo.u-szeged.hu*
[9]*Eötvös University, Inst. of Chemistry, 1117 Budapest, Pázmány P. s. 1/a, Hungary*
[10]*University of Johannesburg, Department of Geology, 2600 Auckland Park, Johannesburg, South Africa*
[11]*Department of Geology & Meteorology, Environmental Analytical & Geoanalytical Research Group, Szentágothai Research Centre, University of Pécs, 7624 Pécs, Ifjúság útja 6 and 20, Hungary*
[12]*Eötvös University, Dept. Mineralogy, H-1117 Budapest, Pázmány P. s. 1/c*

[*]corresponding author

Highlights

^{10}Be data of siderite concretions for comparison with other rock types and meteorites

High resolution mineralogical, geochemical data of siderite surface phase transition

Comparison of transitional effects of weathering or heating on siderite exposed surface

Characterization and ^{10}Be content of iron carbonate concretions for genetic aspects - Weathering, desert varnish or burning: rim effects in iron carbonate concretions

Márta Polgári[1,2*], Szaniszló Bérczi[3], Kazuho Horiuchi[4], Hiroyuki Matsuzaki[5], Tibor Kovács[6], Sándor Józsa[7], Zsolt Bendő[7], Krisztián Fintor[8], József Fekete[1], Zoltán Homonnay[9], Ernő Kuzmann[9], Arnold Gucsik[10], Ildikó Gyollai[1], János Kovács[11], István Dódony[12]

[1]*Research Center for Astronomy and Geosciences, Geobiomineralization and Astrobiological Research Group, Institute for Geology and Geochemistry, Hungarian Academy of Sciences, 1112 Budapest, Budaörsi út. 45, Hungary, e-mail: rodokrozit@gmail.com*
[2]*Eszterházy Károly University, Dept. of Physical Geography and Geoinformatics, Leánka str. 6, 3300 Eger, Hungary*
[3]*Eötvös University, Faculty of Science, Dept. of Materials Physics, Cosmic Materials Space Res. Group, 1117 Budapest, Pázmány P. s. 1/a. Hungary, e-mail: berczi szani@caesar.elte.hu*
[4]*Graduate School of Science and Technology, Hirosaki University, 3, Bunkyo-chou, Hirosaki, Aomori 036-8561, Japan, e-mmail: kh@cc.hirosaki-u.ac.jp*
[5]*Micro Analysis Laboratory, Tandem accelerator (MALT), The University Museum, The University of Tokyo, 2-11-16, Yayoi, Bunkyo-ku, Tokyo 113-0032, Japan, e-mail: hmatsu@um.u-tokyo.ac.jp*
[6]*Institute of Radiochemistry and Radioecology, University of Pannonia, Egyetem Str. 10, Veszprém, H-8200, Hungary, Phone: +36 88 624-789, Fax: +36 88 624-178, e-mail: kt@almos.uni-pannon.hu*
[7]*Eötvös University, Dept. Petrology and Geochemistry, 1117 Budapest, Pázmány P. s. 1/c.*
[8]*Szeged University, Department of Mineralogy, Geochemistry and Petrology, Egyetem str. 2-6, 6702 Szeged, Hungary, e-mail: palm@geo.u-szeged.hu*
[9]*Eötvös University, Inst. of Chemistry, 1117 Budapest, Pázmány P. s. 1/a, Hungary*
[10]*University of Johannesburg, Department of Geology, 2600 Auckland Park, Johannesburg, South Africa*
[11]*Department of Geology & Meteorology, Environmental Analytical & Geoanalytical Research Group, Szentágothai Research Centre, University of Pécs, 7624 Pécs, Ifjúság útja 6 and 20, Hungary*
[12]*Eötvös University, Dept. Mineralogy, H-1117 Budapest, Pázmány P. s. 1/c*

[*]corresponding author

Abstract

Three iron carbonate (siderite) sedimentary concretions were investigated from Nagykovácsi, Uri and Délegyháza, Hungary. Comparative petrological, mineralogical, geochemical and isotopic studies were carried out on identifying possible source rocks and effects of the glaze-like exposed surface of the concretions. The samples are microbially mediated siderite concretions with embedded metamorphous and igneous mineral clasts, and

have specific rim belts characterized by semi-concentric outer Fe-oxide layer, fluffy pyrite-rich outer belt and siderite inner part. The cross section of the Fe-carbonate concretions is investigated by independent methodologies in order to identify their rim effects. Their surficial oxide layers are witness of degassing of the exposed surface caused most probably by elevated temperatures. The inner rim pyrite belt in the concretions excludes longer staying in wet surface environment. Microtextural and mineralogical features do not support desert varnish formation. ^{10}Be nuclide values of the Nagykovácsi and Uri concretions stand far over the level of terrestrial in situ cosmogenic nuclides, but they are in accord of the lowest region for meteorites. Though the data are not conclusive to confirm any kind of known origin, they are contradictional, and open possibilities for a scenario of terrestrial meteorite origin.

Key words: iron-carbonate concretions, siderite, microbial, ^{10}Be content, heated rim minerals, weathering vs. heating effects.

1. Introduction

1.1 Terrestrial radiogenic nuclides

Rocks standing on the surface suffer changes, which cause transformations of exposed surface in components like microtexture, mineralogy, chemistry and isotopic composition, resulting outer rim. We overview all these changes in a multihierarchical comparative analyses in order to distinguish three different ways of transformations: weathering, desert varnish formation or burning at highly elevated temperature. In order to strengthen distinction by the exposition time, ^{10}Be, and ^{14}C contents were also determined. Among commonly measured long lived terrestrial cosmogenic isotopes ^{10}Be is routinely used in geological and geomorphological investigations, as well as in meteorite research. The primary cosmic ray generates secondary

radiation, which results numerous so called terrestrial cosmogenic radiogenic nuclides in the atmosphere and in the rocks and sediments exposed at the surface of the Earth (lithosphere) via nuclear reactions such as ^{3}He, ^{14}C, ^{39}Ar, ^{36}Cl, ^{26}Al, ^{10}Be, ^{32}Si, ^{21}Ne, ^{41}Ca (Wagner, 1998). The half life of ^{10}Be is 1,387,000 yr (Chmeleff et al., 2010; Korschinek et al., 2010) and it is used for exposure dating of rocks, soils, ice cores and also for meteorites. Concentration in cosmogenic nuclides in minerals depends among others on exposure time, latitude, altitude, topography, type of mineral, organic matter content and type of cosmogenic nuclide.

1.2 Desert varnish

Fourteen different types of coatings cover rock surfaces in every terrestrial weathering environment altering the appearance of the underlying landform (Dorn, 2013). Rock varnish (often called "desert varnish") is a paper-thin mixture of about two-thirds clay minerals cemented to the host rock by typically one-fifth manganese and iron oxyhydroxides. Upon examination with secondary and backscattered electron microscopy, the accretionary nature of rock varnish becomes obvious, as does its basic layered texture imposed by clay minerals (Dorn, 2008). The major elements are O, H, Si, Al, and Fe in approximately equal abundance with Mn. Varnish Mn:Fe ratios vary from less than 1:1 to over 50:1, in contrast with Mn:Fe ratios of about 1:60 in the Earth's crust. Concentrations of over 80% Mn in focused spots occur on budding bacteria forms (Dorn, 1998). Varnish minerals were originally reported to be amorphous (Engel and Sharp, 1958), with goethite (Scheffer et al., 1963) and ferric chamosite (Washburn, 1969) as important components. Seminal research conducted with infrared spectroscopy, X-ray diffraction and electron microscopy revealed that the bulk of rock varnish is composed of clay minerals (Potter and Rossman, 1979), dominantly illite, montmorillonite, and mixed-layer illite-montmorillonite. As previously noted, the layering seen in varnish at all scales reflects this clay

mineralogy. Subsequent research has confirmed the dominance of clay minerals (Dorn, 1998, 2008; Krinsley, 1998; Dorn and Krinsley, 2011).

1.3 Siderite

Two iron-carbonate (siderite, $FeCO_3$) concretions of exotic outlook were investigated, Nagykovácsi (Nk) and Úri, and also sedimentary siderite concretions and fragments as counterparts from Délegyháza, Hungary, in order to determine probable origin and fate of these objects. Our paper is focused on the characteristic effects, which were observed in the surface and boundary transitional zone of sample set.

Two independent methodologies were carried on using complex multihierarchical interpretation of data: (i) high resolution petrological, mineralogical, geochemical, isotopic and micro-textural consideration, and (ii) ^{10}Be cosmogenic nuclide determination.

Here, we show that the complex dataset can trace the transformational events in the exposed surface of the iron-carbonate concretions in their texture, mineralogy, chemistry and isotopic composition.

Why siderite? Thinking about the chance to recognize terrestrial originated "meteorites" on the surface, the possible existence of which is raised in the literature (Melosh and Tonks, 1993; Simms, 2011), siderite looks to be the best candidate. Via atmospheric heating magmatic and metamorphic rocks get a melted fusion crust, which is very similar to silicate meteorites. Among sedimentary rocks the most common are carbonates (limestone, dolomite), claystones and sandstone, the last too are often soft. Limestone ($CaCO_3$) and dolomite [$(CaMgCO_3)_2$] suffer degassing of the exposed surface on heat effect, similarly to siderite, but its color asks for macroscopic attention (shiny brown appearance), and the carbon isotopic and mineralogical changes can prove degassing. The macroscopic features of limestone and dolomite do not differ much from the original rock after degassing causing difficulties in identification of their origin and recognition on the surface.

Among the aims of our study was the answering of those questions whether the routinely used methodologies can distinguish siderite objects with various origin from each other convincingly, or not. Further, whether the rim effects on the exposed surfaces of the concretions can be distinguished convincingly according to formation processes including weathering, desert varnish coating formation, or burning (degassing) at highly elevated temperatures. Last but not least, we provide high resolution data on exposed surfaces (surface and boundary transitional zones) of siderite samples, which are scarce in literature.

2. Samples and methods

2.1 Samples

The *Nagykovácsi (Nk)* sample was collected at Nagykovácsi village, the Úri sample at Úri village (Fig. 1). The motivation of sampling was the exotic occurrence of the samples. The Nk shows a pale, shiny, brownish-grayish color (Fig2A). Its ellipsoidal shape has 3.8 cm x 3.4 cm x 2.6 cm in size. Its mass is 66.65 g.

The *Úri*, is very similar to Nk, characterized also by pale brownish-grayish color. Its ellipsoidal shape has 5.2 cm x 3.2 cm x 2.8 cm in size. Its mass is 79.9 g. The samples are covered by small thumbprint indentations (resembling to regmaglypts). Basic data and the used methods on the samples are summarized in Table 1 and Figure 2.

Danube pebbles (DH) were collected in pebble querries near the river Danube, where they are common constituents in the sediments of the ancient Danube (*Délegyháza*, Fig. 1). They are shapeless with variable size dimension from a few cm to some tens cm (Fig. 2A). It is shapeless, on some regions it is covered by small thumbprint indentations (resembling to regmaglypts), somewhere covered by dark-yellow brown rim. Fine-grained matrix with

137 embedded mineral clasts is very similar to Nk and Úri (Supporting Information hereafter SI. 1-
138 3).

139 The samples have a shiny glaze-like cover consisting of Fe-oxide, which defends inner
140 parts of the samples from transitional, among them weathering processes (e.g. pyrite and
141 siderite).

142 **2.2 Methods**

143 Mineral composition was identified by X-ray powder diffraction (XRD) at Eötvös
144 University Dept. Mineralogy, Budapest (Philips diffractometer (PW 1710) with carbon
145 monochromator and Cu Kα radiation), and at Institute for Geological and Geochemical
146 Research, Budapest. Mineral composition was determined on randomly oriented powdered
147 samples by semi-quantitative phase analysis according to the modified method of Bárdossy et al.
148 (1980), using previously defined intensity factors.

149 ^{57}Fe Mössbauer spectra of powered subsamples (Nk-4ab, Nk-3ab-D, Nk-3ab-T) were
150 recorded by conventional Mössbauer spectrometers (WISSEL and HAS Institute for Technical
151 Physics and Material Sciences, Budapest) working in constant acceleration mode in transmission
152 geometry at 293 K and between 20 K and 200 K. A closed circuit refrigerator based cryostat
153 (APD) was used for the low temperature measurements. A 50 mCi activity ^{57}Co(Rh) source
154 supplied the gamma rays for the measurements. The isomer shifts were given relatively to α-Fe.
155 The evaluation of the Mössbauer spectra were carried out via the least squares fitting of
156 Lorentzians by the help of the MOSSWINN program.

157 Raman spectroscopy for micro-mineralogy and organic matter content was made on a
158 representative selected thin section (Nk-2a). Thermo Scientific DXR Raman Microscope was
159 used, with a 532 nm (green) diode pumped solid-state (DPSS) laser with a Nd-YAG source

160 crystal. Measurements were made with 1mW laser power, 50x objective lens in confocal mode
161 (aperture 25 μm pinhole). Acquisition time was 10 min and spectral resolution was ~2 cm^{-1} at
162 each measurement (Szeged University, Hungary). Diagram of peak height vs analytical spot
163 number of each of the 5 phases along the Raman scanned section was calculated. Intensities were
164 normalized to the highest peak for each spectra. The following Raman bands were used for
165 normalization: siderite: ~1083 cm^{-1}; hematite: ~225 cm^{-1}; pyrite: ~380 cm^{-1}; quartz: ~463 cm^{-1};
166 carbonaceous matter: ~1586 cm^{-1}.

167 Optical microscopy was made by NIKON ECLIPSE 600 rock microscope at Institute for
168 Geology and Geochemistry, Budapest.

169 Thermogravimetric (TG) and differential thermal analyses (DTA) were accomplished
170 using a Derivatograph-Q 1500-D instrument at Institute for Geology and Geochemistry,
171 Budapest. Measurement conditions were as follows: approximately 250 mg of samples were
172 heated from 20°C up to 1000°C in a corundum crucible under quartz glass. Meanwhile TG
173 sensitivity was 200 mg and heating rate was 10°C per minute in air-atmosphere. Al_2O_3 was used
174 as reference material. Processing of TG, DTG and DTA curves was carried out with MOM
175 Winder 6.0 software.

176 SEM-EDS was used to determine microtextural features and mineral composition on
177 samples by an AMRAY 1830 SEM equipped with EDAX PV9800 EDS detector, at Eötvös
178 Univ. Dept. Petrology and Geochemistry, Budapest. Conditions of analyses were the following:
179 accelerating voltage 20 kV, beam current 1 nA, electron beam diameter: ~ 50 nm (focused
180 beam), measurement time 100 sec lifetime. Amelia # AS5010-AB albite, MAD-10 orthoclase,
181 Glen Innes, Australia, C. M. Taylor Company kaersutite, LP-6 biotite, C. M. Taylor Company
182 diopside international standards were used.

SEM-FIB – EBSD was used on sample Nk-3ba, using a Quanta 3D FEG (FEI) EDAX-TSL-OIM type equipment, a method ETD, EBSD TSL-OIM Data coll. 5.31 and OIM analysis, carried on 20 kV, 120 pA, 9.8 mm working distance, EDT and vCD detectors measuring conditions, at ELTE Univ. Dept. Physics of Materials, Budapest.

Carbonate samples were prepared and C-14 AMS analysed in the Hertelendi Laboratory of Institute of Nuclear Research HAS, Debrecen. Carbon-dioxide was extracted from the carbonate sample chips using 85% phosphoric acid in a vacuum tight two finger glass flask (75 degree Celsius, 2 hours). The CO_2 produced from the carbonate content of the sample was cleaned by a cryogenic gas purification system. Total amount of released carbon was measured in a calibrated known volume on room temperature by the accurate CO_2 sample gas pressure measurement (+/- 0.3% rel. error). The purified carbon-dioxide was converted into AMS graphite target using the sealed tube graphitization method (Rinyu et al., 2013). A split part of the purified CO_2 was used for stable carbon and oxygen isotope ratio ($\delta^{13}O$ and $\delta^{18}O$ vs. PDB) measurement using a Finnigan Delta XP^{plus} stable isotope ratio mass spectrometer. The C-14 measurements were performed by the MICADAS type AMS at Hertelendi Lab, Debrecen (Synal et al., 2007, Molnár et al., 2013). Measurement time and conditions were set to collect at least 500,000 net counts for every single target. The overall C-14 measurement uncertainty for each sample is below 3‰, including normalization, background subtraction and counting statistics.

Cosmogenic ^{10}Be concentration (in the matrix siderite) was determined on the homogenized powders of the Nk and Uri using Accelerator Mass Spectrometry (AMS) at the Micro Analysis Laboratory, Tandem accelerator (MALT), The University of Tokyo (Matzusaki et al., 2004). The sample pretreatments were carried out at the paleoenvironmental and cosmogenic nuclide laboratory of Hirosaki University. Each 100 µg of the sample was spiked with a 150 µg of ^{9}Be carrier and dissolved in a hot 6M HCl (with 0.5% H_2O_2) solution. Ion

exchange separations were then performed to isolate the beryllium fraction, followed by the precipitation of $Be(OH)_2$ using NH_3(aq.). The precipitates were converted to BeO by heating in a microwave crucible. The BeO was mixed well with Nb powder and pressed into a copper cathode for AMS. The measured $^{10}Be/^{9}Be$ ratios ($1.3–3.1\times10^{-12}$) were calibrated using standard material KNB5-2 (8.56×10^{-12}; Nishiizumi et al., 2007). The $^{10}Be/^{9}Be$ ratio of the process blank was 5×10^{-15}.

Before the ^{10}Be measuremenst the main nuclides were measured using an ICP-MS instrument Agilent 7500. Prior to ICP-MS analyses, standard solutions were prepared from SPEX multi-element plasma standard (Spex CertiPrep, NJ, USA) at 0, 50, 100, 500, and 2500 ppt to derive a calibration curve. To check the accuracy of the calibration, two standard samples were used. The samples were dried at 110°C in the oven to constant weight. The samples were then digested in TeflonTM PFA pressure decomposition vessels in a microwave unit (MLS 1200 mega, Milestones, Italy) using an acid mixture of HNO_3, $HClO_4$, and HF, and high purity water (Milli-Q water purification system). After the samples were completely digested, they were transferred into Teflon beakers and evaporated to dryness on a hot plate (Sahoo et al., 2013).

3. Results

3.1 Macroscopic and microscopic features

The first cut surface observations showed baked rims around a shiny, pale yellowish-brown, very fine grain sized, homogenous sedimentary inner portion (Fig. 2B). In binocular microscope the darker outer baked rims show a few mm thick region in which the color gradually changes from the inner yellowish brown to the outer darker brown rim (Fig. 2BC, SI. 1-3AB).

The SEM-analyzed textural features of the Nk, Úri and DH show strong similarities (Fig. 2D). The clasts are embedded in the fine grained siderite matrix without contact zone, and the texture becomes more and more porous according to increasing quantity of Fe-oxide, and a thin Fe-rich covering occurs around the grains. In the case of Nk remnants of a thin Fe-oxide-rich outer rim occur (SI. 1D, exposed surface siderite and Fe-oxide with clasts, with different magnifications).

The microtexture of the Nk, Úri and DH is similar in the inner part and the exposed surface, in spite of the color differences (Fig. 2C, SI. 1-3B). The very fine grained iron-carbonate (siderite) matrix shows a texture resembling filamentous microbial one, where the filaments have an inner pearl-necklace-like texture (Fig. 2CD, SI. 1-3BC). The fine structure of the matrix, the pyrite and Fe-oxide phases can be seen on SI. 1Dbcd.

The Nk, Úri and DH have a concentric character, which occurs in the above mentioned exposed surface (its thickness is inhomogeneous, but very thin, 1-2 mm). Between the exposed surface and the inner part there is a transitional zone (in color) with variable thickness (average 2-3 mm), which contains disseminated pyrite grains in great number. These pyrite grains are very small and have irregular snowflake shape (SI. 1B, SI. 1Cabcef, SI. 1Dd).

3.2 Mineralogical composition

XRD, Raman, Mössbauer and SEM-EDS investigations determined that the main mineral, forming the inner part of Nk, Úri and DH is iron-carbonate ($FeCO_3$, the mineral siderite, Table 1). The exposed surfaces also contain a considerable amount of Fe-oxide (hematite).

The Mössbauer results revealed that in the exposed surface of the Nk iron occurs in siderite (78 %), in hematite (16 %) and in pyrite (6 %) (Kuzmann et al., 1998; Stevens et al., 2005) (SI. 1De1e2). The hematite is an indicator mineral of the possible heating temperature,

254 which resulted around 370 ºC in our samples during decomposition of iron-carbonate in the
255 exposed surface.

256 Typical ^{57}Fe Mössbauer spectra, recorded at 293K and 20K, of Nk sample (subsample
257 No. NK3ab-T) are shown in SI. 1De1e2. The 293K spectrum was decomposed into two doublets
258 (SI. 1De1). The major doublet is the fingerprint of siderite, based on its characteristic Mössbauer
259 parameters (Stevens et al., 2005). The minor doublet can be assigned to pyrite and
260 superparamagnetic iron oxide (Stevens et al., 2005). The 20K spectrum of was decomposed into
261 2 doublets and 2 sextets (SI. 1De2). The major doublet and the minor sextet belong to siderite,
262 which partly exists in magnetic state at the temperature of the measurement (Forester and Koon,
263 1969). The well resolved major sextet is assigned to superparamagnetic hematite, while the
264 minor doublet can be associated with pyrite (Stevens et al., 2005). The somewhat smaller
265 hyperfine field of the major sextet than usually characteristic for hematite, and can indicate Mn
266 incorporation into the hematite. The Mössbauer results revealed that, in the exposed surface of
267 Nk, iron occurs in siderite (78%), in superparamagnetic hematite (16%) with grain size estimated
268 smaller than 25 nm (Kuzmann et al, 1998) and in pyrite (6%).

269 Raman-spectroscopy confirmed the siderite matrix as composition and variable debris
270 (rutile, feldspar, muscovite, pyrrhotite, quartz, anatase, Table 1, SI. 4). Disseminated organic
271 matter was also determined in the form of amorphous carbon (SI. 1Dfgh). The Raman scanned
272 section from the inner part towards the exposed surface reflects the change of mineral
273 composition from siderite to hematite-wüstite-magnetite and pyrite as well as variable amount of
274 the parent siderite (SI. 1Dfh). Pyrrhotite was also determined in both Nk and DH. Series of
275 spectra from exposed surface to inner part (SI. 1Dh) show negative shift of carbonate major
276 peaks and broadening, which can be caused by decomposition. The broad peak near 650 cm^{-1} is
277 wüstite, which indicate temperature above 800°C. Also, hematite/wüstite and magnetite occur in

exposed surface. Hematite occur with heavily disordered, almost amorphous structure. Such structure is produced under elevated heat effect conditions (e.g. laser beam heating, or during heating in the furnace). Raman measurements were carried on with caution concerninng the effect of laser beam heating.

SEM-EDS determined siderite, and hematite in the degassed outer surface part. Composition of various clasts were also determined (quartz, dolomite, albite, alkaline feldspar, chlorite, chloritoide, mica, pyrite, monazite, zircon, magnetite, ilmenite, titanomagnetite, rutile, amphibole, epidote, staurolite, bastnäsite, apatite, pyroxene, barite and rarely rock clasts of sandstone [quartz grains embedded in sericite, ilmenit-muscovite-epidote] and quartzite, are "suspended"). These minerals reflect a magmatic-metamorphic background source area. The amout of mineral clast is around 7-10 v% of the texture.

DTA-DTG investigations of Nk showed that the siderite (and probably pyrite) content is around 35 %, and the ankerite content is around 5 %. The thermal decomposition of the sample started at 310 °C and the main transformation occurred between 310-370 °C. This supports the Nk being on a temperature up to 310 °C (Table 1).

The DH sample also exhibits similar results on thermal decomposition temperature interval (310-370 °C). Its inner part contains siderite and pyrite (72-74 %), and ankerite (3.5 %), while its exposed surface contains more siderite + pyrite (82 %) and less ankerite (2.7 %) (Table 1).

3.3 Geochemistry

The matrix siderite of Úri and Nk contains FeO as main component (FeO: 73.35-85.83 wt. %), a considerable amount of Mn (MnO: 6.30-13.98 wt. %) and Ca (CaO: 5.90-11.62 wt. %)

and less Mg (MgO: 0.45-1.37 wt. %) (Table 1, SI. 1DF, SI. 2CD). The degassed outer surface part contain 89.11 wt. % FeO, 6.39 wt. % MnO, 2.98 wt. % CaO and 1.52 wt. % MgO.

The bulk geochemical composition of the matrix material and mineral fragments of DH are summarized in Table 1 and SI. 3B-D. Matrix is high Mn-, moderate Ca-, and low Mg-bearing siderite with inhomogeneous composition (FeO: 74.47-76.22 wt. %; MnO: 13.08-13.66 wt. %; CaO: 10.13-11.51 wt. %; MgO: 0.51-1.27 wt. %).

Carbonate carbon concentration of the bulk samples in Nk varied between 7.1 - 8.4 wt. % (inner part) and much less, only 5.3 wt. % in the exposed surface, determined via ^{14}C activity measurement.

Carbonate carbon concentration of the bulk samples in Úri varied between 8.6 wt. % (inner part) and less, only 7.5 wt. % in the exposed surface, determined via ^{14}C activity measurement.

Comparing the chemical composition of samples, the Úri and Nk show strong similarities in the composition of matrix siderite and also of the clast minerals composition. The high amount of Ti-bearing minerals (ilmenite, titanomagnetite, rutile and anatase) is characteristic.

Besides main elements, Ni, Ba, Rb, Sr, Zr, La, Ce, Nd were determined via pilot measurements by XRF, and PGAA (Table 1).

According to carbon and oxygen isotope studies, the $\delta^{13}C_{PDB}$ values in the exposed surface of Úri and Nk were -9.3 to -7.65 ± 0.10 ‰ on average, while the inner part showed -10.60 to -9.5 ± 0.10 ‰. The $\delta^{18}O_{PDB}$ values were uniform at both parts, -4.5 ± 0.1 ‰. The $\delta^{13}C_{PDB}$ value of the inner separated organic carbon was -26.6 ‰ (Table 1).

Exposed surface of DH showed $\delta^{13}C_{PDB}$ -9.4 ‰, while its inner part was -9.94 ‰ (Table 1). The $\delta^{18}O_{PDB}$ values were similar at both parts, -4.0 to – 3.8 ± 0.1 ‰.

Till now a pilot study concerning the ^{14}C activity was determined in a bulk powder sample of the inner part and exposed surface of the Úri and Nk samples. The ^{14}C activity is (C-14 pMC abs) 1.01 (inner part) and 2.23 (exposed surface) for Úri. The ^{14}C activity is (C-14 pMC abs) 1.06 (inner part) and 11.96 (exposed surface) for NK**.** The ^{14}C activity on the bulk of DH is (C-14 pMC abs) 2.14 (Table 1).

Concentration of cosmogenic nuclide ^{10}Be was measured in our Nk and Úri samples. These values are the following: Nk $1.28 \pm 0.05 \times 10^8$ atoms/g, and Úri $2.71 \pm 0.09 \times 10^8$ atoms/g (Table 1).

4. Discussion

Here we discuss the interpretation of the measurements of Nk, Úri and DH in a multihierarchical level system analysis. The benefit of this strategy is that all measurements are boundary conditions for datasets of other one specific hierarchy level measurements. As a consequence of this boundary condition one type of measurement alone cannot determine the origin of the materials system analyzed, and consensus in the mutually corresponding data system – coming from all hierarchy levels – is needed for the final conclusion (SI. 5).

4.1 Origin and source of concretions

Based on mineralogical, isotopic and textural evidences, the formation conditions of siderite can be estimated (Fig. 2, SI. 5). The early diagenetic formation via microbial mediation in suboxic Fe^{3+} reduction zone is the most probable. This process is very common on Earth in natural aquatic sedimentary environments. Under suboxic and neutral-slightly alkaline conditions, Fe^{3+} phase is reduced while organic matter is oxidized via microbial mediation, and a part of the carbon of the organic material mineralizes in the form of Fe-carbonate (Sharma and

348 Clayton, 1965; Hudson, 1977; Konhauser, 1998). Light carbon enrichment in samples (-10.60 ‰
349 $\delta^{13}C_{PDB}$) supports this scenario as well as the very fine, homogeneous grain size, and the
350 amorphous carbonaceous matter in the sample. To achieve early diagenetic siderite, a precursor
351 Fe-oxide phase together with accumulated reactive organic matter has to be supposed. Micro-
352 textural characteristics of the samples resemble mineralized filamentous microbial forms, where
353 the filaments have an inner pearl-necklace-like texture (Frankel and Bazylinski, 2003; Beukes
354 and Gutzmer, 2008) (Fig. 2C).

355 Background sedimentation was most probably wind supported very fine grained
356 magmatic-metamorphic mineral (rarely rock fragment) debris contribution. Applying a
357 calculation based on low T rhodochrosite laboratory experiments to our oxygen isotopic data
358 show, that a temperature between 18-44 °C can be supposed during formation (Kim et al., 2009).

359 The sedimentary (carbonate-siderite) origin and the elevated heat effect („low
360 temperature originated sedimentary rock vs. elevated heat effect" contradiction) of samples if
361 they are not metamorphosed raised the main question: what kind of scenarios may result in such
362 rocks samples.

363 Concretions similar to the studied samples occur, however, no heat effect investigation
364 has been carried out on them. In the transitional part towards the inner part of the samples,
365 numerous fine grained snowflake-like pyrites occur, which zone has an irregular boundary.

366

367 **4.2 Possibility of weathering model of the concretions**

368 Being in oxic conditions for a long time, fine-grained sedimentary siderite is not stable, it
369 oxidizes to limonite (goethite), which weathering process would be more intense in aquatic
370 environment (Senkayi et al., 1986). In the transitional part towards the inner part of the samples,
371 numerous fine grained snowflake-like pyrites occur, which zone has an irregular boundary. This

pyrite excludes any supergene weathering processes, because in such a case pyrite would oxidize to limonite, and sulfuric acids destroy the material, and a soft, clay-bearing brown outer part would be formed, which is missing. The pyrite formed most probably via heat effect from inhomogenously disseminated organic material. These mineral stability considerations exclude the weathering origin of the exposed surface.

4.3 Desert varnish formation

Though the mineral composition of the exposed surface can fit with desert varnish composition in general (hematite, goethite; Potter and Rossman, 1979; Krinsley, 1998; Dorn, 2008; Dorn and Krinsley, 2011), Mn-oxide is missing in the samples, which constituent is common in the varnish (McKeown and Post, 2001; DiGregorio, 2005; Dorn, 2008). The surface of the Nk and Uri nodules exhibit fingerprint-decorated relief, shiny glaze-like outer appereance, similarly to desert varnish. However, this similarity is only a premature (first glance) observation, because mineral composition does not fit for the two types, as desert varnish is composed mainly from clay minerals, which is not the case in our samples.

Microbial mediation in the formation of desert varnish is raised and generally accepted (Dorn and Oberlander, 1981; Palmer et al., 1986; Nagy et al., 1991; Kuhlman et al., 2008; Esposito et al., 2015), but the microtextural features of those microbial activities result different ones as those observed in our samples. However, the microtexture of the exposed surfaces do not support the desert varnish forming scenario, as stromatolite-like, micro-laminated features were not observed (Dorn, 1984; Liu and Broecker, 2000; Goldsmith et al., 2014). The filamentous microtexture, which is characteristic in the inner matrix material can be traced in the exposed surface, too.

Similar siderite concretions were investigated from sandstone formations from the ancient Danube sediments, and reported as evidences of desert crust (Fábián et al., 2004). Recently it has been held that the desertification of Pannonian Basin corresponds to the Messinian Salinity Crisis. A comparison of samples with desert varnish collected NE of Budapest (Mogyoród site), Tapolca Basin, Keszthely Hills and Hassi Zegdou (Algeria), Maktar (Tunesia) supports the desert theory of those samples. Fábián et al. (2004) based their results on macroscopic similarities, X-ray fluorescence (XRF) analyses for main-and trace elements and thermal analyses (TG, DTG) for mineralogy. Though their investigations were not as high resolution in the case of the exposed surfaces as in the recent study, the detailed comparison is not possible. They concluded that during drier climatic periods i.e. Late Miocene, Early Pliocene desert climate as well as Pleistocene glacials the material transport of the winds played an important role in the formation of siderite concretions with exotic outlook, but their verification is not convincing.

4.4 Evidence of heating

It is worth to summarize the thermal stamps measured on the concretions. For Nk the DTA results showed that the sample did not suffer heat effects larger than 310 ^{o}C. For DH and Nk the sulfide component besides pyrite was identified as pyrrhotite by Raman spectroscopy, which is known as a mineral of high tepmerature origin. In the exposed surface of the Nk and DH, the cross section line measurements of Raman spectroscopy identified also wüstite (FeO), a mineral of high temperature origin, and hematite with heavily disordered, almost amorphous structure. Mössbauer measurements also determined the peculiar characteristics of hematite as superparamagnetic hematite with grain size estimated smaller than 25 nm on independent sample. On the other hand, via the decomposition experiment of iron-carbonate by gradual

heating, Wang et al, (2011) observed the beginning of decomposition at heating temperature around 370 ºC. This means that if outer heat effect transformed the exposed surface region of the concretions, then the hematite is an indicator mineral of this heating temperature of 370 ºC or more in our samples during decomposition of iron-carbonate in the exposed surface (Wang et al, 2011). This scenario for the exposed surface is in accord with the high temperature structure of a part of the sulfides (pyrrhotite), wüstite and the heavily disordered structure of the hematite, too.

The staying in terrestrial atmosphere caused degassing of exposed surface and the chemical, mineralogical and isotopic modifications are also the consequences of an effect, which looks like elevated temperature. The mineralogy of the exposed surfaces of the samples were significantly modified, which modification is difficult to explain under normal surface temperature including the extreme desert conditions. Below the exposed surface layer the original siderite looks to have been thermally decomposed to Fe-oxide (poorly crystallized hematite, and/or goethite, and wüstite), with escape of CO_2 (degassing) (Raman, XRD, Mössbauer and DTA results). The Fe-oxide represents shiny, glaze-like rusty brown color causing a well visible exposed surface zone, while in the case of the limestone and dolostone, the degassing products (CaO and MgO) have similar color to the original carbonate (grayish). It seems that this glaze-like oxide surface zone defended the inner part of the samples from weathering. The lack of a melting crust can be attributed to the high melting temperature of FeO (1566 ºC for hematite; Ganesh et al., 2012). We have to take into consideration the conversion of FeO to Fe-carbonate based on hygroscopic features (Fig. 1De) or the remnant phase of parent siderite, as Raman and Mössbauer spectroscopy determined siderite together with hematite. The highly porous microtexture was also detected in the exposed surface of the samples. The degassing zone, visible by optical microscopy and SEM, was about 2 mm. The changes in the chemical composition in the form of enrichment of FeO was also detected by SEM-EDS (89.11

wt. %). On the basis of inorganic C content, the concentration of siderite drops from ~81.2 % to ~51.2 % from the sample core to the exposed surface, confirming the depletion of carbonate with around 30 wt. % loss. We were able to analyse the carbon isotopic signatures on different zones (inner part and exposed surface). These measurements indicate that the exposed surface experienced a $\delta^{13}C_{PDB}$ increase (-10.60 ‰ to -7.65 ‰ for Nk, -9.5 ‰ to -9.3 ‰ for Úri, -9.94 ‰ to -9.4 ‰ for DH) respectively, causing a concentric isotopic change.

After the proposed heating effects a more negative value could form via ^{13}C escape (degassing) in accordance with kinetic isotopic fractionation having accompanied by thermal degradation of the siderite during heating, but later the surface effect of atmospheric CO_2 (+7 ‰ $\delta^{13}C_{PDB}$) via conversion of FeO to Fe-carbonate under cooling surface conditions could cause the observed isotopic signature (Wittkop et al., 2014). The exposed surface also differs from the central portions in their C-14 pMC values. Concerning the $\delta^{18}O_{PDB}$ values, - 4.5 ‰ was detected both in the inner part and in the exposed surface for Nk, and -3.8 ‰ for the exposed surface of DH, while its inner part represent – 4.0 ‰**.** A secondary siderite formation via reaction with atmospheric CO_2 ($\delta^{18}O_{VSMOW}$ ~ +41 ‰) would be expected to increase the bulk $\delta^{18}O$ value of the sample as predominant effect.

Summarizing our results, a good agreement can be observed in data about heating up of our siderite concretions and the heating experiment by Wang et al. (2011), which supports our suggested scenario of heating up our samples in atmospheric conditions.

4.5 ^{10}Be cosmogenic radiogenic nuclide content of the Úri and Nk samples

Concerning terrestrial siderite only very few Be-isotopy data can be found in literature, only ferromanganese crusts composed of siderite and rhodochrosite ($MnCO_3$) were measured in modern oceans (Kastner, 1999). According to Graham et al. (2004), the ^{10}Be concentration of

ferromanganese nodules in a sediment core from the SW-Pacific Ocean varies between 2.0-141.8 x 10^8 atoms/gram. The ^{10}Be concentration of the deep-sea ferromanganese crusts varies in wide intervals from the equatorial Atlantic Ocean (2.95-488 x 10^8 atoms/gram), and North Pacific Ocean (20.4-479 x 10^8 atoms/gram) (Ku et al., 1982). Ferromanganese crust concentration data obtained by Segl et al. (1984) from the Central Pacific Ocean varies between 2.9-232 x 10^8 atoms/gram, the highest concentration occurs at the surface of the crust, the lowest value occurs in 3.8 cm depth.

For comparison from the highest to the lowest ^{10}Be content rocks we placed the ^{10}Be data of Nk and Úri among selected meteorites, among them stony and iron meteorites and terrestrial in situ cosmogenic nuclides produced within minerals at, or close to the surface on the Earth (Fig. 3A). The triggering mechanism of the ^{10}Be nuclide generation is different for meteorites, which were exposed to interplanetary cosmic radiation, and for terrestrial in situ cosmogenic nuclides produced within minerals at, or close to the surface on the Earth, which are also affected by the cosmic radiation, although in a different intensity causing much much less values. Meteorites have the largest ^{10}Be content and our Nk and Úri samples are standing between them and terrestrial in situ cosmogenic nuclides produced within minerals (Fig. 3A). Nk and Úri have been measured for the first time for their ^{10}Be content. Nk and Uri has ^{10}Be content with two orders of magnitude higher than for example a terrestrial limestone, a related terrestrial in situ cosmogenic nuclides produced within quartz pebbles, carbonate rocks, and flint (Nishiizumi et al., 1995; Braucher et al., 2005; Codilean et al., 2009; Shakun and Bierman, 2013).

For further comparison we collected data about the tektites (Ma et al., 2004; Koeberl et al., 2011), marine sediments (Ma et al., 2004; Inoue and Tanaka, 1976) and spherules groups (a part of them is supposed to have cosmic origin as micro meteorites) from terrestrial sediments (Fig. 3B) (Nishiizumi et al., 1995). Sediments have ^{10}Be values in a wide range of our and

meteorite data, however, these sediments have different ^{10}Be accumulating mechanisms. It is important to distinguish terrestrial in situ cosmogenic nuclides produced within minerals at/or close to the surface of the Earth, and soft sediments (soils). The concentration of cosmogenic nuclide ^{10}Be in sediments and in soils is continuously increased by the drizzling of ^{10}Be particles from the terrestrial atmosphere attached to also dust particles which are accumulated by their incorporation to the actually forming sediments. This effect influences also the high concentrations of ^{10}Be in tektites (Nishiizumi et al., 1995).

For overviewing our ^{10}Be isotopic data of Nk and Uri concretions we compared them to the widest range of the measured ^{10}Be values. ^{10}Be values of Úri ($2.71 \pm 0.08 \times 10^8$ atoms/g) and Nk ($1.28 \pm 0.05 \times 10^8$ atoms/g) are in the lowest region of meteorites exposed to the cosmic radiation (cca. one fourth of the lowest values of carbonaceous chondrites, and one third of a L4 chondrite (Kring et al., 2001; Nishiizumi and Caffee, 2012), but they stand far over (two decimal order of magnitudes higher) the level of terrestrial in situ cosmogenic nuclides produced within minerals at, or close to the surface of the Earth (Fig. 3AB) (Nishiizumi et al., 1995; Ma et al., 2004; Braucher et al., 2005; Welten et al., 2008; Codilean et al., 2009; Shakun and Bierman, 2013).

As a consequence, only on the base of ^{10}Be concentration we cannot definitively identify the origin of such concretions. These data alone are not diagnostic for the origin of samples: it is crucial to determine the rock quality and its formation and transformation processes.

5. Conclusions

Petrological and geochemical results support that our sample set is of terrestrial low temperature sedimentary origin and very similar to each other. The instrumental measurements

showed that the main masses of our samples similarly were composed from Mn-, Ca-, and Mg-bearing siderite ($FeCO_3$), the fabrics had been originally formed by a very fine grained microbially mediated siderite sedimentary rock, with minor amount of magmatic and metamorphic mineral debris (clasts). We used multihierarchical analyses methodology trying to follow the fate and origin of these individual, terrestrial sedimentary rock samples.

The iron-carbonate samples have suffered changes in their exposed surface rim in the $\delta^{13}C$ and ^{14}C values and modification of the mineralogy of the samples formed Fe-oxide and Fe-sulfide components. We could identify that the exposed surface is most probably the result of considerable heat effect (310-800 °C, minimum estimation), degassing, based on mineral stability of siderite. Parts of siderite have been transformed to hematite, wüstite and pyrite with variable amounts of parent siderite remnants, which process indicates maximum heating for a period with temperatures over 370 °C, which is a little lower than that found by Wang et al. (2011) (464 °C) attributed to the very small grain size and organic matter content of our samples. Mineral composition and paramagnetic Fe-oxide minerals can be temperature (terminal value) indicators. This behavior is basically different from the melted fusion crust of silicate-mineral-bearing rocks. Also, basically different from terrestrial weathering crusts based on mineral stability considerations. The Fe-oxide represents shiny, glaze-like, rusty brown color causing a well visible exposed surface zone, which offers opportunity of an easier recognition, so siderite suffering degassing is an excellent candidate for such identification because its color asks for macroscopic attention, and the carbon isotopic and mineralogical changes can prove degassing processes via atmospheric heating.

As a further confirmation of atmospheric exposure, as a first step, preliminary study of the ^{10}Be cosmogenic nuclides content of our two samples were determined. Variable cosmogenic nuclides are routinly used in terrestrial rocks studies as complex interpretation concerning

539 exposure time, shielding effect, depth of radiation, matrix effect, etc. ^{10}Be data prove that our
540 iron-carbonate rocks have specific irradiation history, which resulted in ^{10}Be content
541 characteristic to the exposure of its minerals at, or close to the surface. Nobody knows whether
542 ^{10}Be in the siderite samples is cosmogenic (produced in space or at the surface of the Earth) or
543 meteoric (atmospheric fallout). So, the ^{10}Be values are within the range of meteoric ^{10}Be in
544 sediments, although, this fact solely cannot exclude the possibility of radiation in space.

545 Our iron-carbonate samples are the first ones which has been interpolated among the ^{10}Be
546 content of rocks with wide range of origin. Our samples exhibit ^{10}Be values which are in the
547 lowest region of the meteorites exposed to cosmic radiation (cca. one fourth of the lowest values
548 of carbonaceous chondrites and one third of a L4 chondrite), but they stand far over (two decimal
549 order of magnitudes higher) the level of rocks measured for terrestrial in situ cosmogenic
550 nuclides produced within minerals at or close to the surface on the Earth. This position leaves
551 open the possibility of space journey related scenario.

552 Though the considerable heat effect and ^{10}Be data are not conclusive to confirm
553 determined origin and fate of our samples, the data do not contradict also with a short space
554 journey scenario.

555 Together with chemical, mineralogical and isotopic modifications on the exposed
556 surfaces of our samples all data witnessed the effect of elevated temperature (degassing). The
557 aim of this study was to offer plausible interpretation for the „sedimentary rock (low temperature
558 origin) vs. elevated heat effect" contradiction, if it is not metamorphosed?

559 However, the real origin and fate of these samples left open questions. Can this mineral
560 assemblage and textural features be formed via simple sedimentary processes, or not? More work
561 in this area is needed, which can open new perspectives in concretion, exposed surface and also
562 meteorite research.

Acknowledgement

The ^{10}Be measurement (KH and HM's work) was supported by a Grant-in-Aid for Scientific Research (A) (No25247082) from the Japan Society for the Promotion of Science. XRF preliminary data are appreciated to O. Csorba (Eötvös University). We thank I. Futó Institute for Nuclear Research, Debrecen, for stable C and O measurements, K. Havancsák, G. Varga and Z. Dankházi for SEM. We thank M. Balla for INAA data, Sz. Nagy for Raman measurements, M. Molnár for stable C and O and radiogenic C-14 data, Hertelendi Laboratory of Institute of Nuclear Research HAS, Debrecen, Hungary, and K. Kiss and M. Földvári for DTA-TG measurements and data interpretation, Institute for Geology and Geochemistry and Hungarian Geological Institute, Hungary. The comments of unknown reviewers are highly appreciated.

6. References

Ammon, K., Masarik, J., Leya, I., 2009. New model calculations for the production rates of cosmogenic nuclides in iron meteorites. Meteorit. Planet. Sci. 44, 485-503. http://dx.doi.org/10.1111/j.1945-5100.2009.tb00746.x

Bárdossy G., Bottyán, L., Gadó, P., Griger, Á., Sasvári, J., 1980. Automated quantitative phase analysis of bauxites. Am. Mineral. 65, 135-141.

Beukes, N.J., Gutzmer, J., 2008. Origin and paleoenvironmental significance of major iron formations at the Archean-Paleoproterozoic boundary. Rev. Econ. Geol. 15, 5-47.

Braucher, R., Benedetti, L., Bourlès, D.L., Brown, E.T., Chardon, D., 2005. Use of in situ-produced 10Be in carbonate-rich environments: A first attempt. Geochim. Cosmochim. Acta 69, 1473–1478. http://dx.doi.org/10.1016/j.gca.2004.09.010

Chmeleff, J., von Blanckenburg, F., Kossert, K., Jakob, D., 2010. Determination of the 10Be half-life by multicollector ICP-MS and liquid scintillation counting. Nucl. Instrum. Meth. B 268, 192-199. http://dx.doi.org/10.1016/j.nimb.2009.09.012

Codilean, A.T., Fabel, D., Fenton, C.R., Bishop, P., Xu, S., 2009. Grain size dependency of cosmogenic nuclide concentrations in alluvial sediment in an arid zone catchment. Geophys. Res. Abstr. 11, EGU 2009-5321-1.

591 DiGregorio, B.E., 2005. Rock varnish and the manganese oxide connection. Anal. Chem. 77, 433
592 A-438 A.

593 Dorn, R.I., 1984. Cause and implications of rock varnish microchemical laminations. Nature
594 310, 767-770. http://dx.doi.org/10.1038/310767a0

595 Dorn, R.I., 1998. Rock coatings, Elsevier, Amsterdam. http://dx.doi.org/10.1016/S0928-
596 2025(98)80000

597 Dorn, R.I., 2008. Rock Varnish, in: Nash, D.J., McLaren, S.J., (Eds.), Geochemical Sediments
598 and Landscapes. Wiley-Blackwell, Oxford, pp. 246-297.
599 http://dx.doi.org/10.1002/9780470712917.ch8

600 Dorn, R.I., 2013. Rock coatings, in: Shroder, J., Pope, G.A., (Eds.), Treatise on Geomorphology.
601 Academic Press, San Diego, CA, vol. 4, Weathering and Soils Geomorphology, pp. 70–
602 97. http://dx.doi.org/10.1016/B978-0-12-374739-6.00066-X

603 Dorn, R.I., Krinsley, D., 2011. Spatial, temporal and geographic considerations of the problem of
604 rock varnish diagenesis. Geomorphology 130, 91-99.
605 http://dx.doi.org/10.1016/j.geomorph.2011.02.002

606 Dorn, R.I., Oberlander, T.M., 1981. Microbial origin of desert varnish. Science 213, 1245-
607 http://dx.doi.org/1247. 10.1126/science.213.4513.1245

608 Engel, C.G., Sharp, R.S., 1958. Chemical data on desert varnish. Geol. Soc. Am. Bull. 69, 487-
609 518. http://dx.doi.org/10.1130/0016-7606(1958)69[487:CDODV]2.0.CO;2

610 Esposito, A., Ahmed, E., Ciccazzo, S., Sikorski, J., Overmann, J., Holmström, S.J.M., Brusetti,
611 L., 2015. Comparison of Rock Varnish Bacterial Communities with Surrounding Non-
612 Varnished Rock Surfaces: Taxon-Specific Analysis and Morphological Description.
613 Microb. Ecol. 70, 741-750. http://dx.doi.org/10.1007/s00248-015-0617-4

614 Fábián, Sz. Á., Kovács, J., Nagyváradi, L., Varga, G., 2004. Was there desert climate in the
615 Carpathian Basin, or not? Stud. Geomoph. Carpatho-Balcan. 38, 49–58.

616 Ferko, T.E., Schultz, L., Franke, L., Bogard, D.D., Garrison, D.H., Hutchison, R., Lipschutz,
617 M.E., 2000. Exposure history of the Mocs (L6) chondrite: A study of strewn field
618 samples. Meteorit. Planet. Sci. 35, 1215-1227. http://dx.doi.org/10.1111/j.1945-
619 5100.2000.tb01510.x

620 Ferko, T.E., Wang, M-S., Lipschutz, M.E., 2002. Chemical studies of H chondrites 11.
621 Cosmogenic radionuclides in falls. J. Geophys. Res., 107(E10), 5077.
622 http://dx.doi.org/10.1029/2001JE001527

623 Fink, D., Klein, J., Middleton, R., Vogt, S., Herzog, G.F., Reedy, R.C., 1998. ^{41}Ca, ^{26}Al, and
624 ^{10}Be in lunar basalt 74275 and 10Be in the double drive tube 74002/74001. Geochim.
625 Cosmochim. Acta 62, 2389-2402. http://dx.doi.org/10.1016/S0016-7037(98)00134-3

626 Forester, D.W. and Koon, N.C., 1969. Mössbauer Investigation of Metamagnetic $FeCO_3$, J.
627 Appl. Phys. 40, 1316.

628 Frankel, R.B. Bazylinski, D.A., 2003. Biologically induced mineralization by bacteria. Rev.
629 Mineral. Geochem., 54, 95–114. http://dx.doi.org/10.2113/0540095

630 Ganesh, I., Kumar, P.P., Gupta, A.K., Sekhar, P.S., Radha, K., Padmanabham, G., Sundararajan,
631 G., 2012. Preparation and characterization of Fe-doped TiO2 powders for solar light
632 response and photocatalytic applications. Process. Appl. Ceramics 6, 21-36.

633 Goldsmith, Y., Stein, M., Enzel, Y., 2014. From dust to varnish: Geochemical constraints on
634 rock varnish formation in the Negev Desert, Israel. Geochim. Cosmochim. Acta 126, 97-
635 111. http://dx.doi.org/10.1016/j.gca.2013.10.040

636 Graham, I.J., Carter, R.M., Ditchburn, R.G. and Zondervan, A., 2004. Chronostratigraphy of
637 ODP 181, Site 1121 sediment core (Southwest Pacific Ocean), using 10 Be/9 Be dating
638 of entrapped ferromanganese nodules. Marine Geol. 205(1), 227-247.

639 Graly, J.A., Bierman, P.R., Reusser, L.J., Pavich, M.J., 2010. Meteoric ^{10}Be in soil profiles – A
640 global meta-analysis. Geochim. Cosmochim. Acta 74, 6814-6829.
641 http://dx.doi.org/10.1016/j.gca.2010.08.036

642 Graly, J.A., Reusser, L.J., Bierman, P.R., 2011. Short and long-term delivery rates of meteoric
643 ^{10}Be to terrestrial soils. Earth Planet. Sci. Lett., 302, 329-336.
644 http://dx.doi.org/10.1016/j.epsl.2010.12.020

645 Hudson, J.D., 1977. Stable isotopes and limestone lithification. J. Geol. Soc. London 133, 637–
646 660. http://dx.doi.org/10.1144/gsjgs.133.6.0637

647 Inoue, T., Tanaka, S., 1976. ^{10}Be in Marine Sediments. Earth Planet. Sci. Lett., 29, 155-160.
648 http://dx.doi.org/10.1016/0012-821X(76)90035-2

649 Kastner, M., 1999. Oceanic minerals: Their origin, nature of their environment, and significance.
650 Proc. Natl. Acad. Sci. U S A 96, 3380-3387. http://dx.doi.org/10.1073/pnas.96.7.3380

651 Kim, S.-T., Kang, J.O., Yun, S.-T., O'Neil, J.R., Mucci, A., 2009. Experimental studies of
652 oxygen isotope fractionation between rhodochrosite ($MnCO_3$) and water at low
653 temperatures. Geochim. Cosmochim. Acta 73, 4400–4408.
654 http://dx.doi.org/10.1016/j.gca.2009.04.018

655 Koeberl, C., Nishiizumi, K., Caffee, M.W., Glass, B.P., 2011. Beryllium-10 in Australasian
656 Microtektites. Meteorit. Planet. Sci. Suppl., 46, 5429.

Konhauser, K.O., 1998. Diversity of bacterial iron mineralization. Earth-Sci. Rev. 43, 91–121. http://dx.doi.org/10.1016/S0012-8252(97)00036-6

Korschinek, G., Bergmaier, A., Faestermann, T., Gerstmann, U.C., Knie, K., Rugel, G., Wallner, A., Dillmann, I., Dollinger, G., Von Gostomski, C.L., Kossert, K., 2010. A new value for the half-life of ^{10}Be by heavy-ion elastic recoil detection and liquid scintillation counting. Nucl. Instrum. Meth. B, 268, 187-191. http://dx.doi.org/10.1016/j.nimb.2009.09.020

Kring, D.A., Jull, A.J.T., McHargue, L.R., Bland, P.A., Hill, D.H., Berry, F.J., 2001. Gold Basin meteorite strewn field, Mojave Desert, northwestern Arizona: Relic of a small late Pleistocene impact event. Meteorit. Planet. Sci., 36, 1057-1066. http://dx.doi.org/10.1111/j.1945-5100.2001.tb01944.x

Krinsley, D.H., 1998. Models of rock varnish formation constrained by high resolution transmission electron microscopy. Sedimentology 45, 711-725. http://dx.doi.org/10.1046/j.1365-3091.1998.00172.x

Ku, T.L., Kusakabe, M., Nelson, D.E., Southern, J.R., Korteling, R.G., Vogel, J. and Nowikow, I., 1982. Constancy of oceanic deposition of 10Be as recorded in manganese crusts. Nature 299(16), 240-242.

Kuhlman, K.R., Venkat, P., La Duc, M.T., Kuhlman, G.M., McKay, C.P., 2008. Evidence of a microbial community associated with rock varnish at Yungay, Atacama Desert, Chile. J. Geophys. Res., 113, G04022. http://dx.doi.org/10.1029/2007JG000677

Kuzmann, E., Nagy, S., Vértes, A., Weiszburg, T., Garg, V.K., 1998. Geological and Mineralogical Applications of Mössbauer Spectroscopy. in: Vértes, A., Nagy, S., Süvegh, K., (Eds.), Nuclear Methods in Mineralogy and Geology, Techniques and Applications. Plenum Press, New York, pp. 285–376. http://dx.doi.org/10.1007/978-1-4615-5363-2_7

Liu, T., Broecker, W.S., 2000. How fast does rock varnish grow? Geology 28, 183-186. http://dx.doi.org/10.1130/0091-7613(2000)28<183:HFDRVG>2.0.CO;2

Lundberg, L., Ticich, T., Herzog, G.F., Hughes, T., Ashley, G., Moniot, R.K., Tuniz, C., Kruse, T., Savin, W., 1983. ^{10}Be and Be in the Maurice River-Union Lake System of Southern New Jersey. J. Geophys. Res., 88, 4498-4504. http://dx.doi.org/10.1029/JC088iC07p04498.

Ma, P., Aggrey, K., Tonzola, C., Schnabel, C., de Nicola, P., Herzog, G.F., Wasson, J.T., Glass, B.P., Brown, L., Tera, F., Middleton, R., Klein, J., 2004. Beryllium-10 in Australasian tektites: constraints on the location of the source crater. Geochim. Cosmochim. Acta 68, 3883-3896. http://dx.doi.org/10.1016/j.gca.2004.03.026

690 Matsuzaki, H., Nakano, C., Yamashita, H., Maejima, Y., Miyairi, Y., Wakasa, S., Horiuchi, K.,
691 2004. Current status and future direction of MALT, The University of Tokyo. Nucl.
692 Instrum. Meth. B, 223/224, 92-99. http://dx.doi.org/10.1016/j.nimb.2004.04.022

693 McKeown, D.A., Post, J.E., 2001. Characterization of manganese oxide mineralogy in rock
694 varnish and dendrites using X-ray absorption spectroscopy. Am. Mineral., 86, 701-713.
695 http://dx.doi.org/10.2138/am-2001-5-611

696 Melosh, H.J., Tonks, W.B., 1993. Swapping Rocks: Ejection and Exchange of Surface Material
697 among the Terrestrial Planets. Meteoritics 28, 398–398.

698 Molnár, M., Janovics, R., Major, I., Orsovszki, J., Gönczi, R., Veres, M., Leonard, A.G., Castle,
699 S.M., Lange, T.E., Wacker, L., Hajdas, I., Jull, A.J.T., 2013. Status report of the new
700 AMS ^{14}C sample preparation lab of the Hertelendi laboratory of environmental studies
701 (Debrecen, Hungary). Radiocarbon 55, 665-676.
702 http://dx.doi.org/10.2458/azu_js_rc.55.16394

703 Nagy, B., Nagy, L.A., Rigali, M.J., Jones, W.D., Krinsley, D.H., Sinclair, N.A., 1991. Rock
704 varnish in the Sonoran Desert: microbiologically mediated accumulation of
705 manganiferous sediments. Sedimentology 38, 1153-1171.
706 http://dx.doi.org/10.1111/j.1365-3091.1991.tb00376.x

707 Nishiizumi, K., Caffee, M.W., 2012. Exposure Histories of CI1 and CM1 Carbonaceous
708 Chondrites. Lunar Planet. Sci. 43, #2758.

709 Nishiizumi, K., Arnold, J.R., Brownlee, D.E., Caffee, M.W., Finkel, R.C. and Harvey, R.P.,
710 1995. Beryllium-10 and aluminum-26 in individual cosmic spherules from Antarctica.
711 Meteoritics 30, 728-732. http://dx.doi.org/10.1111/j.1945-5100.1995.tb01170.x

712 Nishiizumi, K., Imamura, M., Caffee, M.W., Southon, J.R., Finkel, R.C., McAninch, J., 2007.
713 Absolute calibration of ^{10}Be AMS standards. Nucl. Instrum. Meth. B, 258, 403-413.
714 http://dx.doi.org/10.1016/j.nimb.2007.01.297

715 Pal, D.K., Tuniz, C., Moniot, R.K., Savin, W., Vajda, S., Kruse, T., 1986. ^{10}Be contents of SNC
716 meteorites, in: Reedy, R.C., Englert, P. (Eds.), Workshop on Cosmogenic Nuclides. LPI
717 Technical Report 86-06, LPI, Houston, pp. 62-63.

718 Pal, D.K., Moniot, R.K., Kruse, T.H., Tuniz, C., Herzog, G.F., 1985. Spallogenic ^{10}Be in the Jilin
719 chondrite. Earth Planet. Sci. Lett., 72, 273-275. http://dx.doi.org/10.1016/0012-
720 821X(85)90012-3

721 Palmer, F.E., Staley, J.T., Murray, R.G.E., Counsell, T., Adams, J.B., 1986. Identification of
722 manganese-oxidizing bacteria from desert varnish. Geomicrobiol. J., 4, 343-360.
723 http://dx.doi.org/10.1080/01490458609385943

724 Potter, R.M., Rossman, G.R., 1979. The manganese- and iron-oxide mineralogy of desert
725 varnish. Chem. Geol. 25, 79-94. http://dx.doi.org/10.1016/0009-2541(79)90085-8

726 Rinyu, L., Molnár, M., Major, I., Nagy, T., Veres, M., Kimák, Á., Wacker, L., Synal, H-A.,
727 2013. Optimization of sealed tube graphitization method for environmental C-14 studies
728 using MICADAS. Nucl. Instrum. Meth. B, 294, 270-275.
729 http://dx.doi.org/10.1016/j.nimb.2012.08.042

730 Sahoo, S.K., Hosoda, M., Prasad, G., Takahashi, H., Sorimachi, A., Ishikawa, T., Tokonami, S.,
731 Uchida, S., 2013. Naturally occurring radionuclides and rare earth elements in weathered
732 Japanese soil samples. Acta Geophys., 61, 876–885. http://dx.doi.org/10.2478/s11600-
733 013-0131-3.

734 Scheffer, F., Meyer, B., Kalk, E., 1963. Biologische ursachen der wüstenlackbildung. Z.
735 Geomorph., N.F., 7, 112-119.

736 Senkayi, A.L., Dixon, J.B., Hossner, L.R., 1986. Todorokite, goethite, and hematite: alteration
737 products of siderite in east Texas lignite overburden. Soil Sci., 142, 36-42.

738 Segl, M., Mangini, A., Bonani, G., Hofmann, H.J., Nessi, M., Suter, M., Wölfli, W., Friedrich,
739 G., Plüger, W.L., Wiechowski, A. and Beer, J., 1984. 10Be-dating of a manganese crust
740 from Central North Pacific and implications for ocean palaeocirculation. Nature
741 309(5968), 540-543.

742 Shakun, J., Bierman, P.R., 2013. A 7 Myr record of Greenland glaciation and erosion from in
743 situ ^{10}Be in marine sediments. American Geophysical Union, Fall Meeting 2013, abstract
744 #C31C-08. http://abstractsearch.agu.org/meetings/2013/FM/C31C-08.html

745 Sharma, T., Clayton, R.N., 1965. Measurement of $^{18}O/^{16}O$ ratios of total oxygen of carbonates.
746 Geochim. Cosmochim. Acta 29, 1347–1354. http://dx.doi.org/10.1016/0016-
747 7037(65)90011-6

748 Simms, M.J., 2011. Where are all the Terrestrial Meteorites? Meteorit. Planet. Sci. 46, Suppl.
749 5474.

750 Stevens, J.G., Khasanov, A.M., Miller, J.W., Pollak, H., Li, Z., 2005. Mössbauer Mineral
751 Handbook. Mössbauer Effect Data Center, University of North Carolina, Asheville.

752 Synal, H.A., Stocker, M., Suter, M., 2007. MICADAS: A new compact radiocarbon AMS
753 system. Nucl. Instrum. Meth. B, 259, 7–13.

754 Wagner, G.A., 1998. Cosmogenic Nuclides, in: Wagner, G.A. (Ed.), Age Determination of
755 Young Rocks and Artifacts. Springer Berlin, Heidelberg, pp. 113-194.
756 http://dx.doi.org/10.1007/978-3-662-03676-1_5

Wang, J., Sakakura, T., Ishizawa, N., Eba, H., 2011. Structural evolution of $FeCO_3$ through decarbonation at elevated tempreatures. Mater. Sci. Eng., 18, 022011. http://dx.doi.org/10.1088/1757-899X/18/2/022011.

Washburn, A.L., 1969. Desert varnish, in: Washburn, A.L. (Ed.), Weathering, Frost Action and Patterned Ground in the Mesters District, Northeast Greenland. Reitzels, Copenhagen, pp. 14-15.

Welten, K.C., Folco, L., Nishiizumi, K., Caffee, M.W., Grimberg, A., Meier, M.M.M., Kober, F., 2008. Meteoritic and bedrock constraints on the glacial history of Frontier Mountain in northern Victoria Land, Antarctica. Earth Planet. Sci. Lett., 270, 308-315. http://dx.doi.org/10.1016/j.epsl.2008.03.052

Wittkop, C., Teranes, J., Lubenow, B., Dean, W.E., 2014. Carbon-and oxygen-stable isotopic signatures of methanogenesis, temperature, and water column stratification in Holocene siderite varves. Chem. Geol., 389, 153-166. http://dx.doi.org/10.1016/j.chemgeo.2014.09.016

The authors confirm that all have been involved with the work, approved the manuscript, and agree to its submission. M.P. and Sz.B. the first two authors have contributed equally to this work, conceived and planned the study, collected the samples, made macroscopic descriptions, thin section microscopy, and summarized data, and interpreted the data and wrote the manuscript K.H. H.M. and T.K. offered ^{10}Be data and interpretation, S.J. (thin section microscopy); Zs.B. (SEM-EDS data and interpretation); K.F. (performed Raman spectroscopy and data interpretation); J.F. (isotope data interpretation and temperature calculation); Z.H. and E.K. (Mössbauer data and interpretation); A.G. and J.K. (interpretation of data); I.Gy. (temperature calculation, mineral stability aspects); E.P.M. (microbial data interpretation); I.D. (performed X-ray powder diffraction measurements and interpretation).

Additional Information

Competing financial interests

The authors declare no competing financial interests.

786

787 **Figure caption**

788

789 **Fig. 1.** Localities of sample sets. Úri (N47°24'59"/E19°31'04"), Nagykovácsi (Nk,
790 N47°34'32"/E18°52'43"), Délegyháza (DH, N47°15'03"/E19°03'41"). The figure was drawn by
791 hand (Sz.B.) and then redrawn by using CorelDraw12 (I.Gy).

792

793 **Fig. 2.** Characteristics of the samples on macroscopic and microscopic level. Macroscopic **(AB)**
794 and microscopic textural features **(CD)** of Nagykovácsi (Nk), Úri and DH samples. **(series C)**
795 (A) brown exposed surface of Nk with pyrite-bearing (black grains) zone with mineral clasts, the
796 matrix material is siderite (1N), (B) brown exposed surface with mineral clasts, the matrix
797 material is siderite, the arrows show signs resembling microbial activity (1N), (C) characteristic
798 micro-texture of siderite matrix resembling filamentous microbial morphology with pearl
799 necklace-like inner texture in the matrix and around the quartz clast (arrows); (**series D**) (a-i)
800 exposed surface of Nk by variable higher magnification of marked areas, light parts are Fe-oxide
801 together with Fe-Mn-Ca-Mg-bearing carbonate (*), embedded siderite (s), arrows show
802 snowflake-like fine-grained pyrite, most of the black clasts are quartz grains (q) (BSE images).
803 For details see SI 1-4.

804

805 **Fig. 3.** Values of the ^{10}Be cosmogenic nuclide content of Nk and Uri samples with comparison of
806 selected meteorites and some terrestrial in situ cosmogenic nuclides produced within minerals at
807 or close to the surface of Earth. **(A)** The Nk and Uri ^{10}Be values are between the meteorites
808 exposed to cosmic radiation and the values of terrestrial in situ cosmogenic nuclides produced
809 within minerals at or close to the surface of the Earth. Our samples exhibit ^{10}Be values in the
810 lowest region of the meteorites exposed to cosmic radiation (cca. one fourth of the lowest values

of carbonaceous chondrites and one third of an L4 chondrite), but they stand far over (two decimal order of magnitudes higher) the level of terrestrial in situ cosmogenic nuclides produced within minerals at or close to the surface of the Earth. The range embraces 5 orders of decimal magnitudes from meteorites to flints in this sequence. **(B)** Values of the ^{10}Be cosmogenic nuclide content of Nk and Uri samples for comparison with sediments. Their ^{10}Be content is continuously increased by the drizzling ^{10}Be particles from the terrestrial atmosphere attached to dust particles which are accumulated by their incorporation to the actually forming sediments. The source of data: **Fig. 3A**. Extraterrestrial general (Ma et al., 2004), Lunar basalt and lunar soil (Fink et al., 1998), Iron meteoroids (Ammon et al., 2009), Meteorite falls (Ferko et al., 2002), Mócs (Ferko et al., 2000), Martian meteorites/SNC (Pal et al., 1986), FRO 01149 H4 chondrite (Welten et al., 2008), Jilin chondrite (Pal et al., 1985), CM1 and CI1 carbonaceous chondrites (Nishiizumi and Caffee, 2012), Gold Basin UA1172,1 (Kring et al., 2001), Nk and Uri (this work), Continental sediments (Shakun and Bierman, 2013), Quartz pebbles (Nishiizumi et al., 1995; Codilean et al., 2009), Calcite and Flint (Braucher et al., 2005); **Fig. 3B**. Tektite (Koeberl et al., 2011), Tektite (Ma et al., 2004), Soil (Ma et al., 2004; Graly et al., 2010, 2011), Riverine (Ma et al., 2004), Bauxite (Ma et al., 2004), Mixed coastal sediments (Ma et al., 2004), Loess paleosol (Ma et al., 2004), Terrigenous marine self (Ma et al., 2004), Lacustrine sed. (Union Lake) (Lundberg et al., 1983; Ma et al., 2004), Marine sediments (Ma et al., 2004), Marine sediments (Samoan) (Inoue and Tanaka, 1976), Hemopelagic sed. (Ma et al., 2004), Terrigenous (Ma et al., 2004), Spherules/Antarctic and Spherules/Deep sea (Nishiizumi et al., 1995). Numbers in brackets show number of samples or number of measurements. The diagrams were consructed by Excel 2013, M.P.

Figure 1

Click here to download Figure: Fig_1.pdf

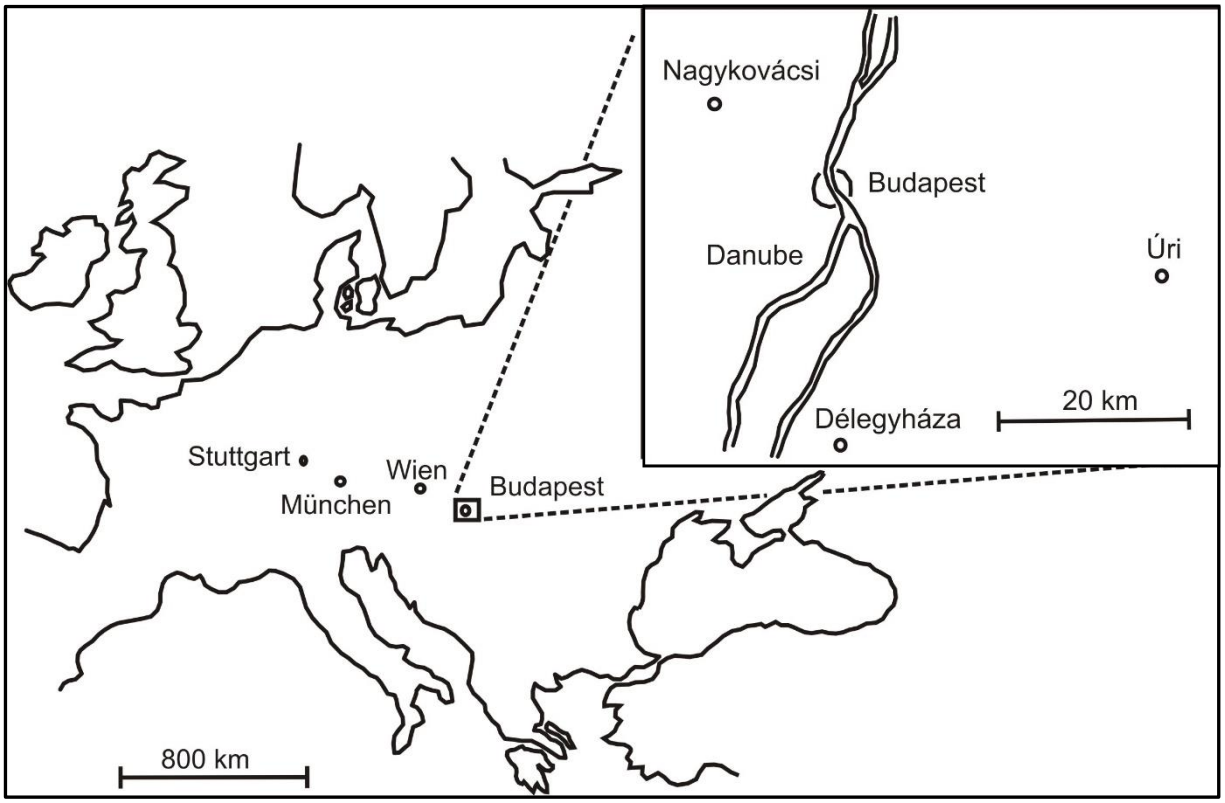

Figure 2

Click here to download Figure: Fig_2.pdf

Fig. 2. Comparison of the three samples on macroscopic and microscopic level

A – hand specimen

NAGYKOVÁCSI (Nk)	ÚRI	DÉLEGYHÁZA (DH)

Scale: 1 cm

B– Polished thin section photos

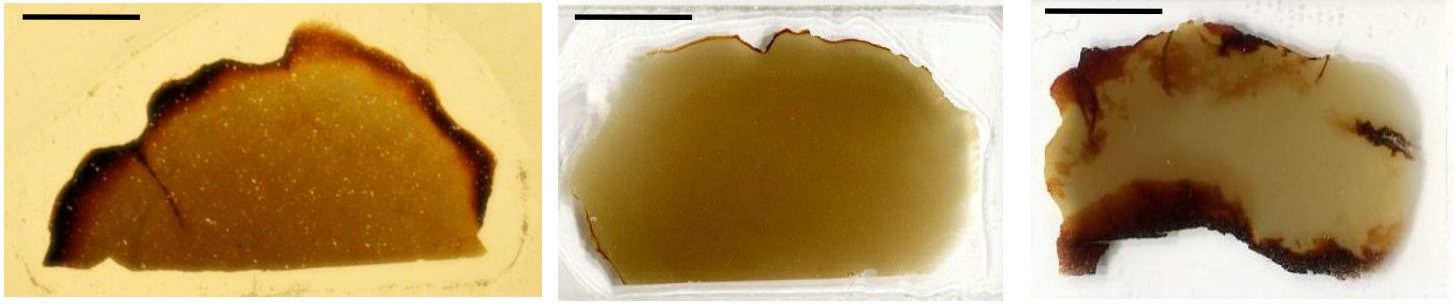

Scale: 1 cm

C – Microtexture (transmitted light photos, optical microscopy)

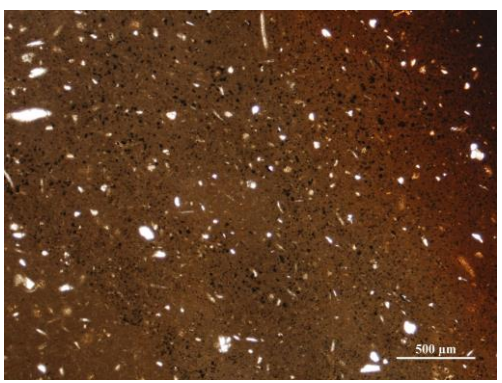

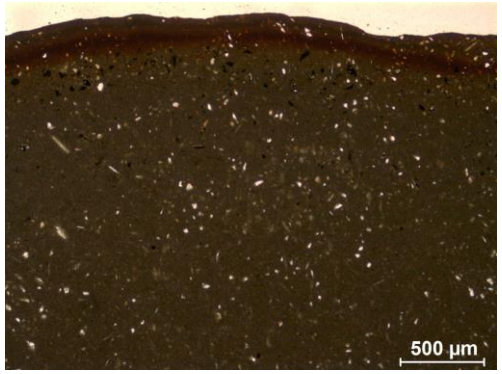

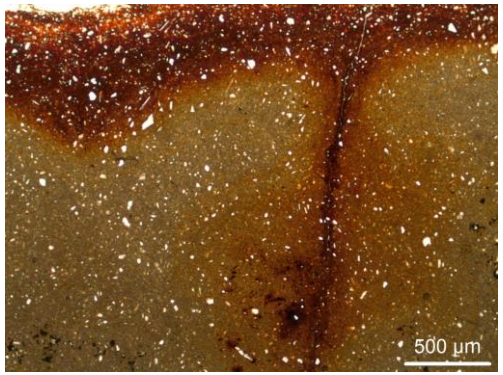

A

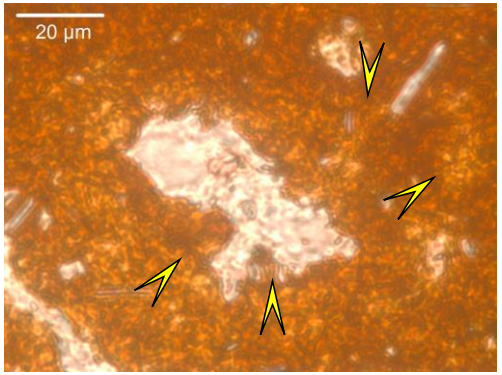

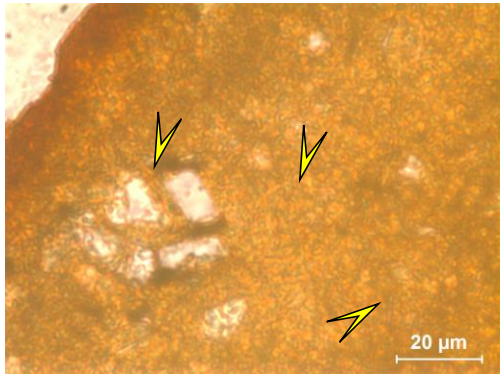

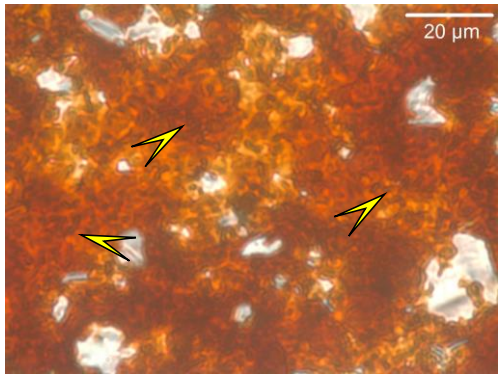

B

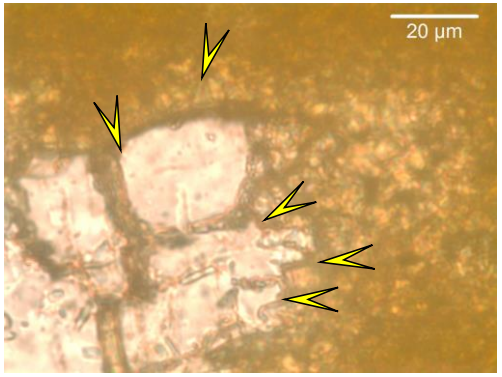

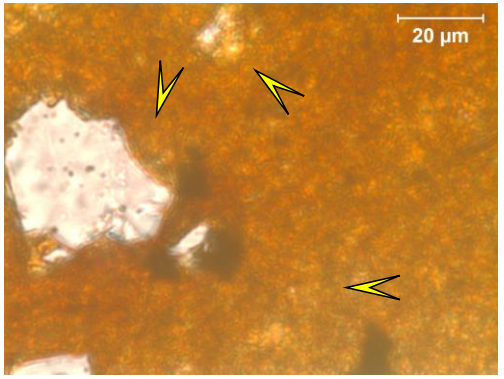

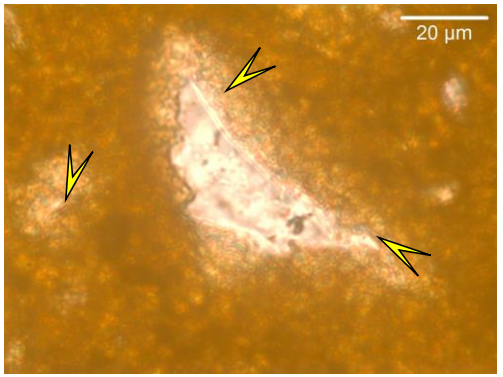

C

D - SEM

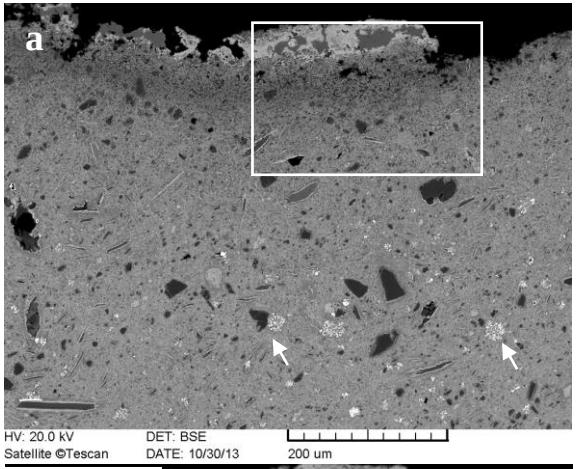
a
HV: 20.0 kV
DET: BSE
Satellite ©Tescan
DATE: 10/30/13
200 um

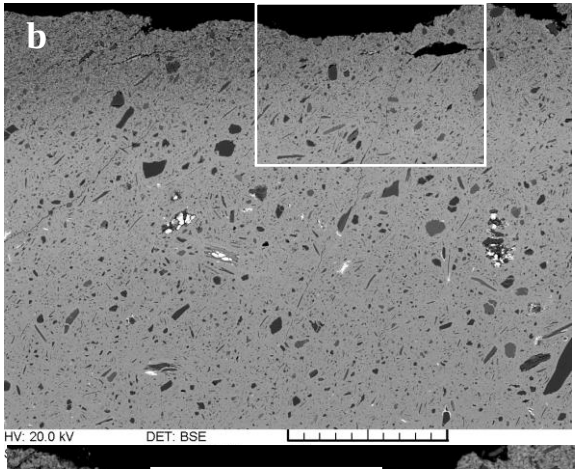
b
HV: 20.0 kV
DET: BSE

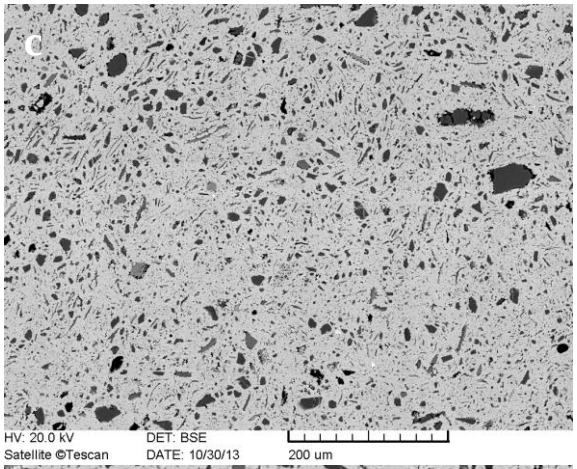
c
HV: 20.0 kV
DET: BSE
Satellite ©Tescan
DATE: 10/30/13
200 um

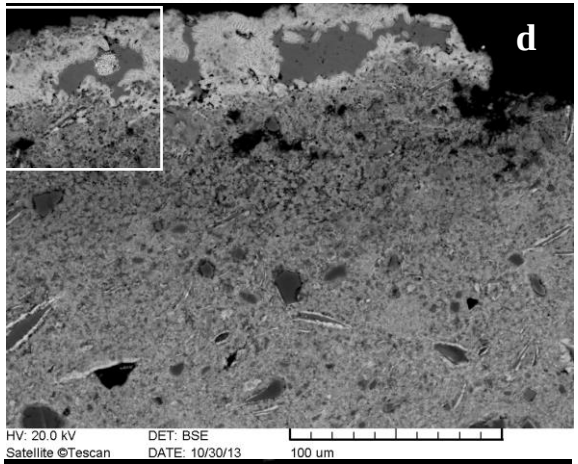
d
HV: 20.0 kV
DET: BSE
Satellite ©Tescan
DATE: 10/30/13
100 um

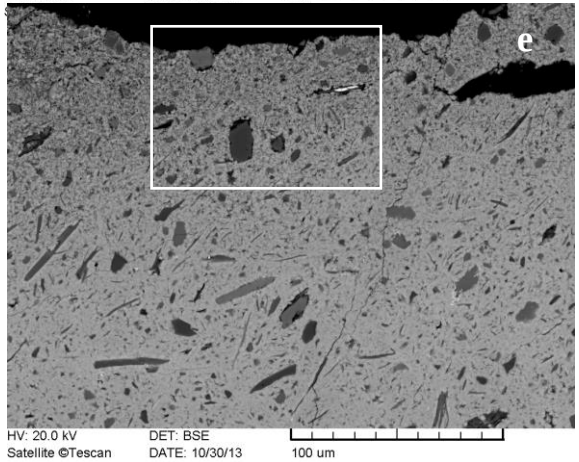
e
HV: 20.0 kV
DET: BSE
Satellite ©Tescan
DATE: 10/30/13
100 um

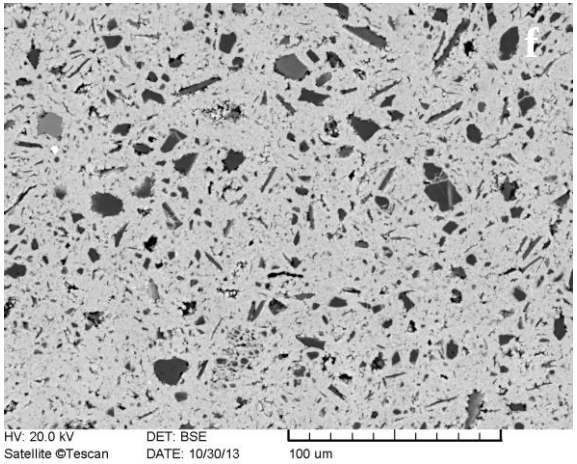
f
HV: 20.0 kV
DET: BSE
Satellite ©Tescan
DATE: 10/30/13
100 um

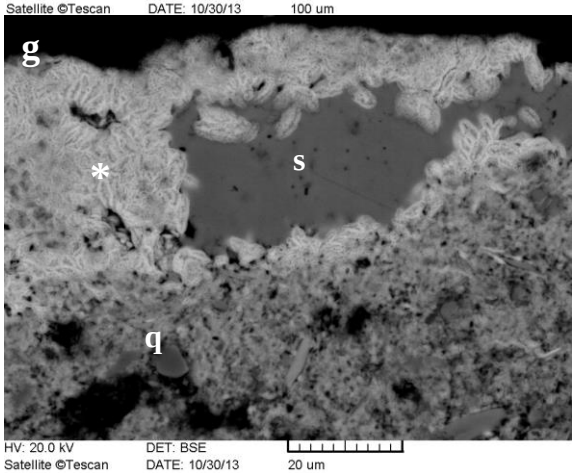
g
*
s
q
HV: 20.0 kV
DET: BSE
Satellite ©Tescan
DATE: 10/30/13
20 um

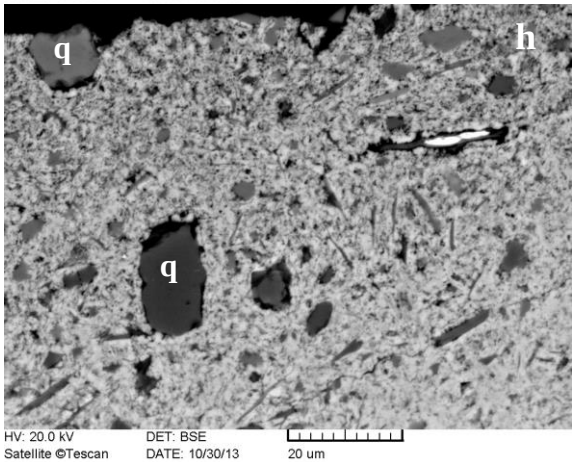
h
q
q
HV: 20.0 kV
DET: BSE
Satellite ©Tescan
DATE: 10/30/13
20 um

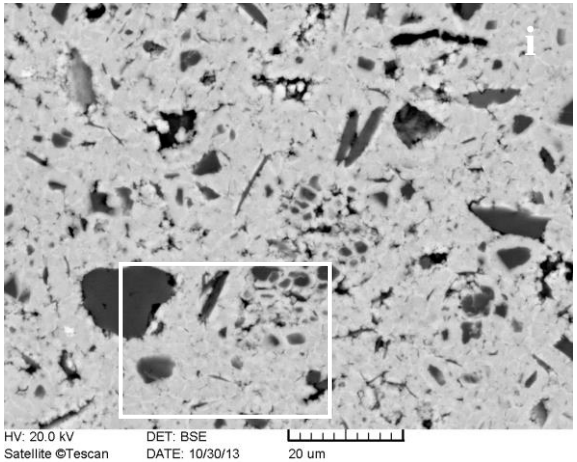
i
HV: 20.0 kV
DET: BSE
Satellite ©Tescan
DATE: 10/30/13
20 um

Figure 3

Click here to download Figure: Fig_3.pdf

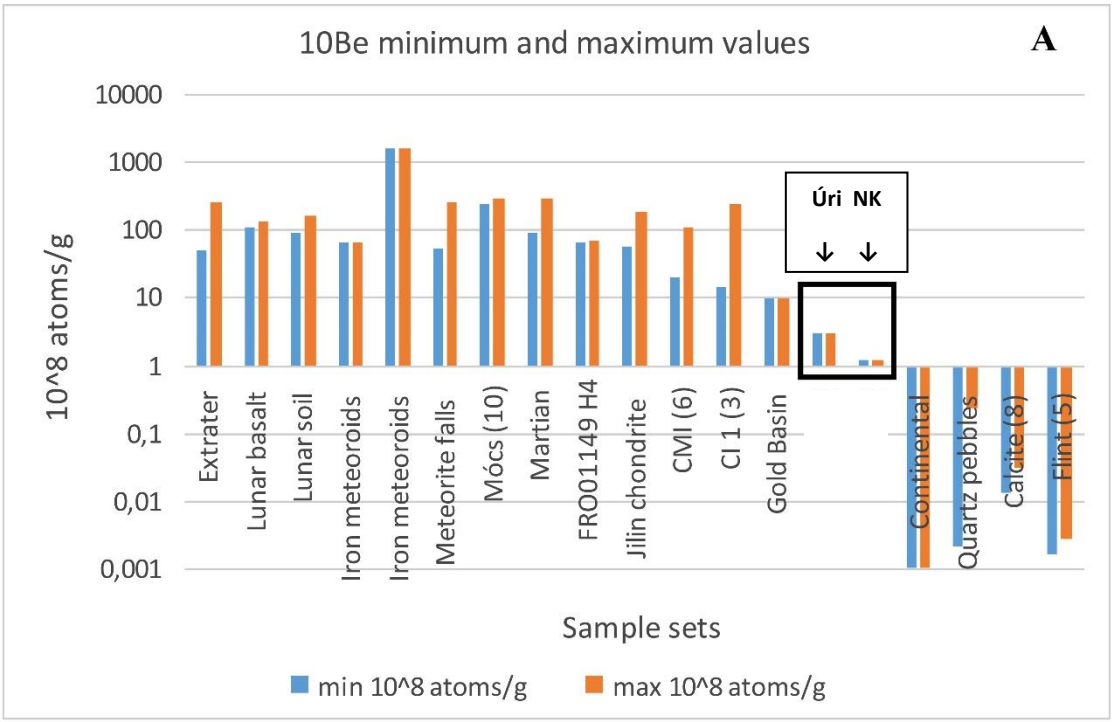

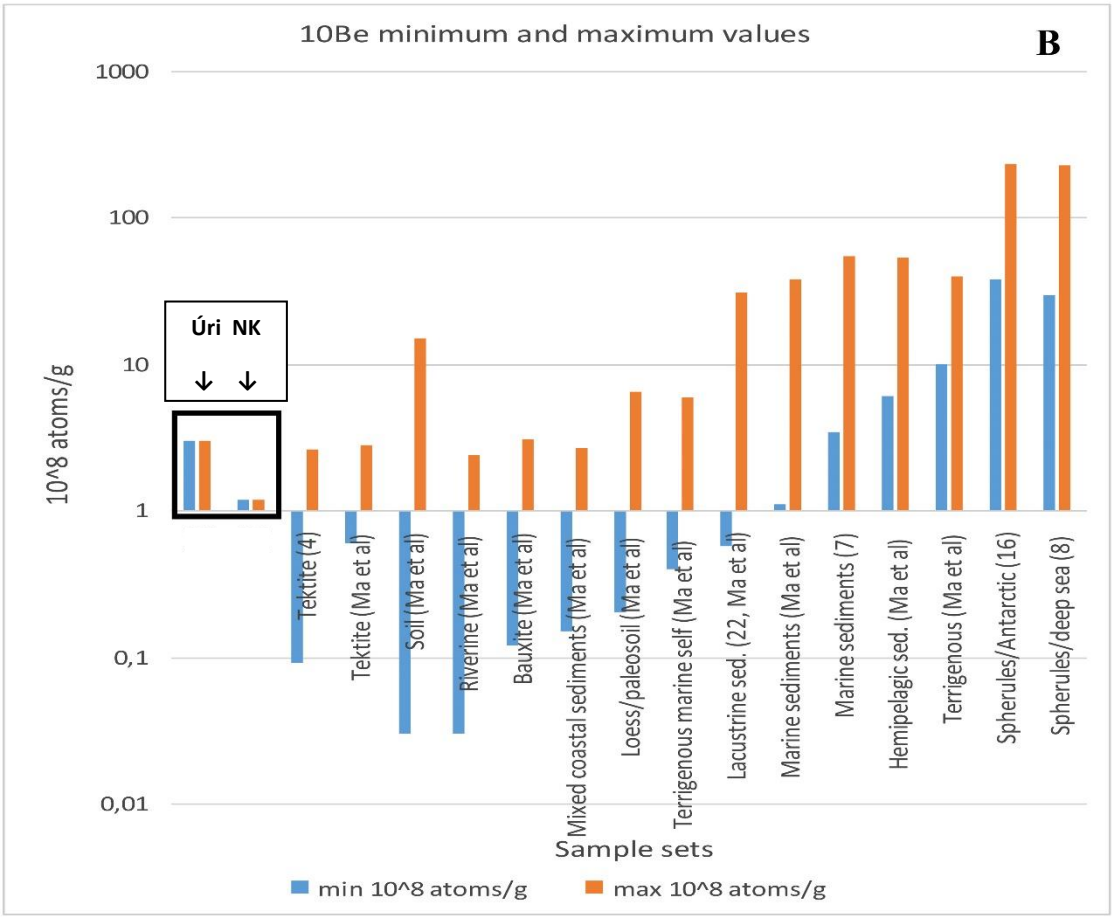

Table 1

Click here to download Table: Table_1.docx

Table 1. Comparison of the Nagykovácsi (Nk), Úri and Danube pebble (DH, Délegyháza) siderite samples

Samples → Features ↓	Nagykovácsi (Nk)	Uri	Délegyháza (DH)
Locality	N47°34'32"/E18°52'43"	N47°24'59"/E19°31'04"	N47°15'03"/E19°03'41"
Occurrence	texture and included clasts are similar to Úri	texture and included clasts are similar to Nk	shapless, variable
Size	3.8cm x 3.4 cm x 2.6 cm (ellipsoidal)	5.2 cm x 3.2 cm x 2.8 cm (ellipsoidal)	variable from a few cm to tens of cm
Total mass	66.65 g	79.90 g	
Average density (calculated) (g/cm^3)	3.4	3.4	3.4
Macroscopic	„cratered" surface, resembling to regmaglypts, brown exposed surface, dark-yellow brown	„cratered" surface, resembling to regmaglypts, brown exposed surface, dark-yellow brown	on some regions „cratered" surface, resembling to regmaglypts somewhere baked shell, dark-yellow brown
Macroscopic section	Fine-grained matrix with embedded mineral clasts	fine-grained matrix with embedded mineral clasts	fine-grained matrix with embedded mineral clasts
Microtexture	similar in the inner part and the brown exposed surface, in spite of the color difference, the very fine grained iron-carbonate matrix shows a texture resembling filamentous microbial one, where the filaments have an inner pearl-necklace-like texture, embedded mineral clasts	similar in the inner part and the brown exposed surface, in spite of the color difference, the very fine grained iron-carbonate matrix shows a texture resembling filamentous microbial one, where the filaments have an inner pearl-necklace-like texture, embedded mineral clasts	similar in the inner part and the baked rim, in spite of the color difference, the very fine grained iron-carbonate matrix shows a texture resembling filamentous microbial one, where the filaments have an inner pearl-necklace-like texture, embedded mineral clasts
Mineralogy (bulk-XRD)	siderite (Mn-bearing), with rhodochrosite	siderite (Mn-bearing), minor quartz	siderite, hematite
Raman mineralogy	siderite matrix, amorphous carbon, rutile, feldspar, muscovite, pyrrhotite, quartz, anatase	no data	siderite matrix, rarely dolomite spots, pyrrhotite, dark brown parts - hematite, carbonate, The main character, the site of the peaks, and the shape of the curve of the spectrum of hematite is almost the same as that of measured in the Nagykovácsi sample. The detrital quartz, anatase, is also occurring together with alkaline feldspar, mica and chlorite, too.
SEM (siderite) composition (wt. %)	FeO: 73.35-85.83 exposed surface: 89.11 MnO: 7.03-13.98 6.39 CaO: 5.90-11.62 2.98 MgO: 1.07-1.23 1.52	FeO: 74.89-84.91 MnO: 6.30-8.46 CaO: 7.41-11.12 MgO: 0.45-1.37	FeO: 74.47-76.22 MnO: 13.08-13.66 CaO: 10.13-11.51 MgO: 0.51-1.27
SEM-EDS (clasts) Composition (wt. %)	quartz, dolomite, albite, alkaline feldspar, chlorite, chloritoide, mica, pyrite, monazite, zircon, magnetite, ilmenite, amphibole, epidote, staurolite, bastnäsite; rarely rock clasts of sandstone (quartz grains embedded in sericite, ilmenit-muscovite-epidote) and quartzite, are "suspended"; the fragments give 5-10 v. % of the texture	quartz, dolomite, albite, alkaline feldspar, chlorite, mica (biotite, muscovite), pyrite, monazite, zircon, ilmenite, amphibole, epidote, apatite, pyroxene, barite (Sr) TiO_2; the fragments give 5-7 v. % of the texture	quartz, dolomite, albite, alkaline feldspar, chlorite, chloritoide, mica, pyrite, monazite, zircon, magnetite, ilmenite, amphibole, epidote, staurolite, bastnäsite; rarely rock clasts of sandstone (quartz grains embedded in sericite, ilmenit-muscovite-epidote) and quartzite, are "suspended"; the fragments give 4-7 v. % of the texture
57 Fe Mössbauer	conclusion: the grain size of the iron-oxide-hydroxide phase is smaller than 25 nanometer (even less than 20 nanometer) (In the	no data	no data

	exposed surface region), it contains siderite (78 %), superparamagnetic hematite (16 %) and pyrite (6 %)		
DTA-DTG	The sample has not survived in its pre-life greater than 310-370 ^{o}C heat impact (In the inner portion of the sample) Siderite+pyrite (35%); ankerite? (5%)	no data	The sample has not survive in its pre-life greater than 310-370 ^{o}C heat impact Inner part: siderite+pyrite (72-74%); ankerite? (3.5%) exposed surface: siderite+pyrite (82%); ankerite? (2.7%)
$\delta^{13}C_{PDB}$ (‰)	-7.65 ± 0.10 (exposed surface) -10.60 ± 0.10 (inner part) -26.6± 0.10 (inner part, separated organic matter)	-9.3 ± 0.10 (exposed surface) -9.5 ± 0.10 (inner part)	-9.4 (exposed surface) -9.94 (inner part)
Carbonate carbon content (wt. %)	5.3 (exposed surface) 7.75 (inner part)	7.5 (exposed surface) 8.6 (inner part)	no data
$\delta^{18}O_{PDB}$(‰)	-4.5 ± 0.10 (exposed surface) -4.5 ± 0.10 (inner part)	no data	-3.8 (exposed surface) -4.0 (iiner part)
C-14 pMC abs ± pMC	11.96 ± 0.17 (exposed surface) 1.06 ± 0.05 (inner part)	2.23 ± 0.10 (exposed surface) 1.01 ± 0.04 (inner part)	2.14 (bulk)
Be-10 x 10^{8} ± atoms/g	1.17 ± 0.05	2.96 ± 0.09	no data
PGAA	El- wt. %: H-0.86; B-0.0031; Al-2.8; Si-5.7; Cl-0.02; K-0.72; Ca-13.1; Ti-0.2; Mn-19.2; Fe-56.5; Co-0.02; Sm-0.00052; Gd-0.0004; Cd-0.0004; Total-100.00	no data	El- wt. %: H-0.52; B-0.0031; Al-1.8; Si-7.6; Cl-0.004; K-0.57; Ca-9.5; Ti-0.3; Mn-13.9; Fe-65.7; Co-0.01; Sm-0.00045; Gd-0.0003; Total-100.00
ICP-MS	El-µg/g(sd): Cr-15.87(0.34); Mn-71927(430); Co-81.93(0,49); Ni-33.52(0.84); Cu-8.56(0.27); Zn-36.7(2.0); Rb-18.48(0.43); Sr-38.68(0.23); Y-22.66(0.13); Cd-1.09(0.14); Cs-1.346(0.014); Ba-143.6(0.9); La-16.3(0.4); Ce-28.5(0.2); Pr-2.56(0.06); Nd-10.67(0.14); Sm-2.14(0.13); Eu-0.49(0.01); Gd-2.11(0.06); Tb-0.37(0.01); Dy-2.16(0.16); Ho-0.42(0.00); Er-1.40(0.04); Tm-0.19(0.01): Yb-1.43(0.07); Lu-0.21(0.01); Pb-5.286(0.078); Bi-0.223(0.004); Th-1.69(0.03); U-2.99(0.03)	El-µg/g(sd): Cr-16.14(0.46); Mn-38669(231); Co-35.23(0.16); Ni-27.31(0.53); Cu-6.03(0.03); Zn-92.1(2.0); Rb-14.20(0.51); Sr-43.24(0.13); Y-50.32(0.17); Cd-0.64(0.24); Cs-1.255(0.006); Ba-190.3(0.5); La-19.9(0.2); Ce-43.0(0.1); Pr-3.96(0.12); Nd-17.90(0.52); Sm-4.26(0.13); Eu-1.11(0.06); Gd-4.79(0.22); Tb-0.99(0.01); Dy-6.14(0.14); Ho-1.24(0.01); Er-4.12(0.04); Tm-0.65(0.02): Yb-4.70(0.05); Lu-0.72(0.04); Pb-10.814(0.044); Bi-0.227(0.003); Th-1.50(0.01); U-11.68(0.09)	no data

Supplementary Material

Click here to download Supplementary Material: SI_160721.pdf